



HAL
open science

Added-value of ensemble prediction system on the quality of solar irradiance probabilistic forecasts

Josselin Le Gal La Salle, Jordi Badosa, Mathieu David, Pierre Pinson,
Philippe Lauret

► To cite this version:

Josselin Le Gal La Salle, Jordi Badosa, Mathieu David, Pierre Pinson, Philippe Lauret. Added-value of ensemble prediction system on the quality of solar irradiance probabilistic forecasts. *Renewable Energy*, 2020, 162, pp.1321-1339. 10.1016/j.renene.2020.07.042 . hal-02952551

HAL Id: hal-02952551

<https://hal.univ-reunion.fr/hal-02952551>

Submitted on 7 Sep 2022

HAL is a multi-disciplinary open access archive for the deposit and dissemination of scientific research documents, whether they are published or not. The documents may come from teaching and research institutions in France or abroad, or from public or private research centers.

L'archive ouverte pluridisciplinaire **HAL**, est destinée au dépôt et à la diffusion de documents scientifiques de niveau recherche, publiés ou non, émanant des établissements d'enseignement et de recherche français ou étrangers, des laboratoires publics ou privés.



Distributed under a Creative Commons Attribution - NonCommercial 4.0 International License

Added-value of Ensemble Prediction System on the quality of solar irradiance probabilistic forecasts

Josselin Le Gal La Salle^a, Jordi Badosa^b, Mathieu David^a, Pierre Pinson^c, Philippe Lauret^a

^a*Université de la Réunion - Laboratoire de Physique et ingénierie mathématique pour l'énergie, l'environnement et le bâtiment (PIMENT), 15 avenue René Cassin, 97715, Saint-Denis Cedex 9, La Réunion, France*

^b*LMD-Laboratoire de météorologie dynamique, Palaiseau, France*

^c*DTU - Technical University of Denmark*

Abstract

Accurate solar forecasts is one of the most effective solution to enhance grid operations. As the solar resource is intrinsically uncertain, a growing interest for solar probabilistic forecasts is observed in the solar research community. In this work, we compare two approaches for the generation of day-ahead solar irradiance probabilistic forecasts. The first class of models termed as deterministic-based models generates probabilistic forecasts from a deterministic value of the irradiance predicted by a Numerical Weather Prediction (NWP) model. The second type of models denoted by ensemble-based models issues probabilistic forecasts through the calibration of an Ensemble Prediction System (EPS) or from information (such as mean and variance) derived from the ensemble. The verification of the probabilistic forecasts is made using a sound framework. A numerical score, the Continuous Ranked Probability Score (CRPS), is used to assess the overall performance of the different models. The decomposition of the CRPS into reliability and resolution provides a further detailed insight into the quality of the probabilistic forecasts. In addition, a new diagnostic tool which evaluates the contribution of the statistical moments of the forecast distributions to the CRPS is proposed. This tool denoted by MC-CRPS allows identifying the characteristics of an ensemble that have an impact on the quality of the probabilistic forecasts. The assessment of the different models is done on several sites experiencing very different climatic conditions. Results show a general superior performance of ensemble-based models as the gain in forecast quality measured by the CRPS ranges from 4% to 16% depending on the site.

Keywords: Day-ahead solar irradiance probabilistic forecast, Ensemble prediction system, Non parametric methods, Ensemble calibration, CRPS

1 Contents

2 1 Introduction

3

*Fully documented templates are available in the elsarticle package on CTAN.

Preprint submitted to Renewable Energy

June 23, 2020

3	2 Building probabilistic forecasts	6
4	2.1 Statistical techniques used to generate probabilistic forecasts	7
5	2.1.1 The linear quantile regression (LQR) technique	7
6	2.1.2 The Analog Ensemble (AnEn) technique	8
7	2.1.3 The Nonhomogeneous truncated Gaussian Regression technique (<i>t_NGR</i>)	9
8	2.1.4 The Nonhomogeneous Regression of Generalized Extreme Value tech-	
9	nique (<i>NR_GEV</i>)	9
10	2.2 Obtaining probabilistic forecasts from deterministic forecasts (Deterministic-	
11	based approach)	11
12	2.3 Obtaining probabilistic forecasts from ensemble forecasts (Ensemble-based	
13	approach)	11
14	2.3.1 From the raw output of ECMWF-EPS	11
15	2.3.2 From information extracted from an EPS	11
16	3 Verification of the probabilistic forecasts	12
17	3.1 Attributes for a skillful probabilistic model	12
18	3.2 CRPS	13
19	3.2.1 Definition	13
20	3.2.2 CRPS Skill Score	13
21	3.2.3 Decomposition of the CRPS	14
22	3.3 Contributions of the statistical moments of the forecast distribution to the	
23	CRPS	14
24	4 Case studies	16
25	4.1 Measurements	16
26	4.2 Forecasts	17
27	5 Results	17
28	5.1 Overall performance of the methods	17
29	5.2 Detailed insight through the decomposition of the CRPS	19
30	5.3 Detailed insight through the CRPS Moments-Contributions	21
31	6 Discussion	22
32	6.1 Deterministic-based approach versus ensemble-based approach	22
33	6.2 Discussion related to CRPS Moments-Contributions	23
34	7 Conclusions	28
35	Appendix A Data quality check	31
36	Appendix B Bias and standard deviation of EPS members distribution	
37	and observations for the six sites	37
38	Appendix C Selection of the optimal α	39

39 1. Introduction

40 Operations of electrical power systems are becoming more challenging as the share of
41 solar energy increases. In particular, due to the intrinsic variability of the solar resource,
42 high penetration of solar power generation into the electrical grid may put in danger the
43 grid supply-demand balance. Energy storage systems (EES) are one of the means used to
44 ensure the grid stability. Notwithstanding, accurate PV power forecasting is a cost-effective
45 way to size and operate ESS optimally. Consequently, PV power forecasts facilitate the
46 large-scale integration of solar energy into the grid. In addition, for energy trading, accurate
47 PV power forecasts are also required because penalties in proportion with the forecast errors
48 are applied.

49 In this study, however, we focus on the global horizontal solar irradiance (GHI) forecasts
50 instead of PV power forecasts. The present work constitutes thus a first step in assessing
51 the contribution of the proposed methodologies for improving the quality of the PV power
52 forecasts and of their potential gain for improved grid operations. Day-ahead GHI forecasts
53 are treated here as they have been considered essential to secure the power grid [1]. More-
54 over, we propose to work on probabilistic forecasting in order to estimate the uncertainty
55 associated to day-ahead GHI forecasts. This additional knowledge permits for instance grid
56 operators to improve their decisions regarding the grid operations. The interested reader can
57 refer to [2] or [3] to understand the benefits of a probabilistic forecast against a deterministic
58 one.

59 Day-ahead GHI forecasts are classically generated by Numerical Weather Predictions
60 models (NWP). For instance, The Integrated Forecasting System (IFS) model of the Eu-
61 ropean Centre of Medium-Range Weather Forecasts (ECMWF) provides day-ahead GHI
62 forecasts [4]. The forecasts can take either the form of a deterministic forecast or an en-
63 semble forecast denoted by the term Ensemble Prediction System (EPS). EPS consists in
64 a set of several perturbed forecasts of irradiance, each representing a possible future state
65 of the atmosphere. If an EPS gives an important information about the uncertainty associ-
66 ated to a forecast, it requires a high computational cost. Thus, the added value of EPS for
67 probabilistic forecasting needs to be determined to justify their computation.

68 We propose below to conduct a bibliographic survey related to day-ahead solar forecasts
69 with a special emphasis on the use of NWP outputs to generate probabilistic forecasts.
70 One of the first approach used to generate day-ahead probabilistic irradiance forecasts was
71 proposed by Lorenz et al. [5]. In this work, a Gaussian distribution of the error of the
72 ECMWF-IFS deterministic irradiance forecast was used to generate prediction intervals.
73 Alessandrini et al. [6] developed an analog statistical method approach applied to a set of
74 explanatory weather variables (GHI, cloud cover, air temperature, etc.) provided by the
75 NWP Regional Atmospheric Modeling System (RAMS) to generate probabilistic PV power
76 forecasts for three solar farms located in Italy. Zamo et al. [7] proposed two statistical
77 approaches to generating probabilistic forecasts of daily PV production from information
78 provided by Météo France's EPS, PEARP. The first approach makes use of the PEARP
79 control member as unique input to quantile regression methods while the second one averages
80 the set of quantiles calculated from each of the 35 members of the PEARP ensemble. Bacher

81 et al. [8] used a weighted quantile regression (WQR) technique to compute up to 24h ahead
82 probabilistic PV forecasts. In addition to lagged PV measurements, the WQR model used
83 also a NWP-based GHI deterministic forecast. Lauret et al. [9] used the IFS model to
84 produce quantile forecasts of solar irradiance and Iversen et al. [10] introduces the idea of
85 modeling uncertainty by stochastic differential equations from a NWP-based deterministic
86 forecast provided by the Danish Meteorological Institute. Bakker et al. [11] proposed a
87 comparison of seven statistical regression models to issue GHI probabilistic forecasts from
88 the deterministic numerical weather prediction (NWP) model HARMONIE-AROME (HA)
89 and the atmospheric composition model CAMS.

90 It must be noted that the above cited works make use of deterministic information
91 extracted from NWP models to generate probabilistic forecasts with the help of statistical
92 techniques like quantile regression or analog ensemble. Others authors like Sperati et al.
93 [12] proceeded differently. In their work, Sperati et al. [12] generated up to 72h probabilistic
94 forecasts from the raw EPS provided by the ECMWF. In this study, two post-processing
95 methods (also called calibration techniques) applied to the initial raw ensemble were used
96 to further improve the quality of the probabilistic forecasts. Massidda and Marrocu [13]
97 went a little bit further and proposed a methodology to combine ECMWF ensemble and
98 the high-resolution IFS deterministic forecast.

99 If we extend our bibliographic survey to the probabilistic predictions of other weather
100 variables such as wind, temperature or precipitation, more publications can be found on
101 how to use information from NWP models to generate probabilistic forecasts. For example,
102 Pinson [14] and Pinson and Madsen [15] suggested a framework for the calibration of wind
103 ensemble forecasts. Junk et al. [16] proposed an original calibration model for wind-speed
104 forecasting applied to ECMWF-EPS based on the combination between Nonhomogeneous
105 Gaussian Regression and Analog Ensemble Models. Likewise, Hamill and Whitaker [17]
106 suggested an adaptation of the analog ensemble technique for the calibration of ensemble
107 precipitation forecast, using the statistical moments of the distribution such as mean and
108 spread of the members as predictors.

109 Wilks [18], followed in his methodology by Williams et al. [19], compared several post-
110 processing techniques of weather EPS forecasts, such as ensemble dressing, Logistic Re-
111 gression, Nonhomogeneous Gaussian Regression (NGR) and Rank-Histogram recalibration.
112 The reader can refer to [20] and [21] for more details regarding the parametric calibration
113 of ensemble forecasts with techniques like NGR with a special emphasis on the choice of the
114 type of the parametric distribution used by the regression technique. Finally, the interested
115 reader should consult the reference book [22], which proposes a summary of the common
116 probabilistic forecasting ensemble-based models with their respective pros and cons.

117 Based on this bibliographic survey, two different approaches for day-ahead GHI proba-
118 bilistic forecasting with the help of NWP models can be identified, which we denoted here
119 by approaches 1 and 2 :

- 120 1. Approach 1 referred herein as *deterministic-based models* : the probabilistic forecast
121 is computed from deterministic NWP predictors with the help of statistical methods.
122 Linear Quantile Regression and Analog Ensemble techniques are particularly attractive

123 to implement this methodology.

- 124 2. Approach 2 referred herein as *ensemble-based models* : the estimation of the forecast
125 is made through the calibration of an EPS or from information (for example mean or
126 spread) inferred from the ensemble. For instance, calibration techniques like Nonho-
127 mogeneous Regression can be used to improve the raw ensemble EPS. Also, methods
128 based on Linear Quantile Regression and Analog methods can be used to produce
129 probabilistic forecasts from the mean and spread of the ensemble.

130 It must be stressed however that, to the best of our knowledge, no previous works have
131 been dedicated to the comparison of the two approaches and particularly in the realm of
132 solar probabilistic forecasts. In this work, our main goal is therefore to assess the relative
133 merits of each approach for day-ahead GHI probabilistic forecasts. Besides, we would like
134 to highlight the possible added-value brought by EPS for probabilistic forecasting. Indeed,
135 it is well known that the generation of such ensemble necessitates high computing capacities
136 compared to a single deterministic forecast that is fed into a statistical method to produce
137 the probabilistic forecasts. More precisely, it should be noted that the calculation cost is
138 not the same to produce only the control member of EPS or the whole set of members.

139 To understand the benefits associated with the usage of EPS, we propose in this paper a
140 sound and consistent methodology to evaluate the respective contribution of each approach.
141 First, the quality appraisal of the different models will be made according the verification
142 framework proposed by Lauret et al. [23]. This framework (which is not consistently pro-
143 posed in the literature) is based on visual diagnostic tools and numerical scores like the
144 Continuous ranked Probability Score (CRPS) which permits to objectively rank the com-
145 peting forecasting methods. However, this classical verification framework is not sufficient to
146 completely explain the contribution of the statistical moments of the forecast distributions
147 to the forecast quality. That is why we propose in a second step a new tool that evaluates
148 the accuracy of all moments of the forecast distribution and its contribution to the CRPS
149 score. We hope that this new diagnostic tool will provide a more in-depth understanding
150 of the performance of each approach. To this end, we evaluate models that generate day-
151 ahead GHI probabilistic forecasts on 6 sites that experience different sky conditions. The
152 probabilistic models are built :

- 153 1. With only the control member of the EPS as a deterministic predictor (deterministic-
154 based approach),
- 155 2. With a deterministic predictor inferred from the whole set of EPS's members. The
156 first statistical moment (mean of the members) can be such a deterministic predictor
157 (ensemble-based approach),
- 158 3. With several predictors inferred from the ensemble like the mean and the variance of
159 the ensemble (ensemble-based approach).

160 We propose the following structure for the paper. Section 2 introduces the different
161 forecasting models while section 3 briefly presents the diagnostic tools used for the verifica-
162 tion of probabilistic forecasts. Section 4 presents the case studies and details the data used
163 to evaluate the different probabilistic models. Section 5 provides a detailed assessment of

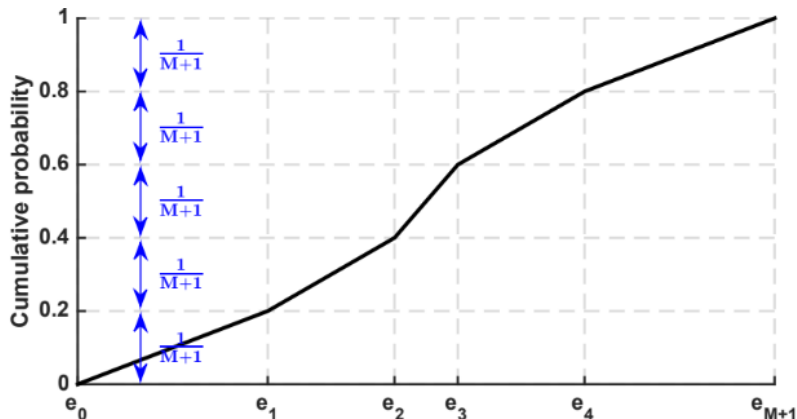


Figure 1: Illustration of an uniform construction of a CDF from an ensemble of $M = 4$ members (e_1, e_2, e_3, e_4). The tails of the CDF are bounded by e_0 and e_{M+1} which correspond to the minimum and the maximum of the climatology.

164 the performance of the different methods. Finally, a discussion will be conducted in sec-
 165 tion 6, trying to understand the pros and cons of each forecasting methods and the factors
 166 impacting the forecast quality.

167 2. Building probabilistic forecasts

168 Regarding probabilistic forecasts of continuous predictand like GHI, a probability state-
 169 ment i.e. either a Probability Distribution Function (PDF) f or a Cumulative Distribution
 170 Function (CDF) F encodes the uncertainty of the forecast. In this work, three ways to
 171 estimate this CDF or PDF are considered: parametric PDFs, discrete quantile estimates of
 172 a CDF via a non-parametric method and CDF derived from EPS.

173 In this study, the EPS is provided by the European Centre of Medium-Range Weather
 174 Forecasts (ECMWF). It corresponds to 50 perturbed members and a control run (unper-
 175 turbed member) [4] that give the cumul of the GHI with a 3 hours time step. This leads
 176 to a total of $M = 51$ members. An EPS can be seen as discrete estimates of a CDF when
 177 they are sorted in ascending order. Lauret et al. [23] discussed three ways to associate these
 178 sorted members to cumulative probabilities. In this work, we chose the uniform distribution
 179 which consists in a uniform spacing of the members and a linear interpolation between the
 180 members. More precisely, this choice assigns a probability mass of $1/(M + 1)$ between two
 181 members and for events that fall outside of the ensemble. Using this definition, the i^{th}
 182 ensemble member can be interpreted as a quantile forecast with a probability level equal
 183 to $\tau = \frac{i}{M+1}$. Put differently, the ECMWF ensemble forecasts are in the form of 51 equally
 184 spaced quantiles with probability levels $\tau = \frac{1}{52}, \frac{2}{52}, \dots, \frac{51}{52}$. This construction is illustrated
 185 in Figure 1, for an EPS with 4 members. In the following, we present first the different
 186 statistical techniques used to estimate the uncertainty of the forecasts. Secondly, we detail
 187 the two approaches introduced in section 1.

188 *2.1. Statistical techniques used to generate probabilistic forecasts*

189 *2.1.1. The linear quantile regression (LQR) technique*

This method estimates the quantiles of the cumulative distribution function F of some response variable Y (also called predictand) by assuming a linear relationship between the quantiles of Y , namely q_τ and a set of explanatory variables X (called predictors):

$$q_\tau = \beta_\tau X + \epsilon, \quad (1)$$

190 where β_τ is a vector of parameters to optimize for each probability level τ and ϵ represents
191 a random error term.

192 Following Koenker [24], the

vector $\hat{\beta}_\tau$ that defines each quantile is obtained as the solution of the following minimization problem:

$$\hat{\beta}_\tau = \arg \min_{\beta} \sum_{i=1}^N \Psi_\tau (Y_i - \beta X_i). \quad (2)$$

193 where N is the number of pairs of observed predictand Y_i , set of predictors X_i taken from
194 the training set. $\Psi_\tau(u)$ is the quantile loss function defined as :

$$\Psi_\tau(u) = \begin{cases} u\tau & \text{if } u \geq 0, \\ u(\tau - 1) & \text{if } u < 0, \end{cases} \quad (3)$$

195 with τ representing the quantile probability level. Hence, in quantile regression, the quantiles
196 are estimated by applying asymmetric weights to the mean absolute error.

197 Thus, the quantity $\hat{q}_\tau = \hat{\beta}_\tau X$ is the estimation of the τ^{th} quantile obtained by the LQR
198 method.

199 It must be noted that the quantile regression method estimates each quantile separately
200 (i.e. the minimization of the quantile loss function is made for each τ separately). As a
201 consequence, one can obtain quantile regression curves that may intersect, i.e $\hat{q}_{\tau_1} > \hat{q}_{\tau_2}$ when
202 $\tau_1 < \tau_2$. To avoid this issue during the model fitting, we used the rearrangement method
203 described by Chernozhukov et al. [25].

204 Figure 2 shows some quantiles estimates of the CDF of the predictand Y (here GHI)
205 as a function of the day-ahead forecasted GHI. Hence, in this case, the predictor X is the
206 predicted irradiance which will be represented in this work either by the ECMWF control
207 member or the mean of the ECMWF ensemble (see Table 2 below). This example shows that
208 the forecast uncertainty depends on the level of the predicted irradiance. More precisely,
209 and as shown by Figure 2, the dispersion of points is lower for values of predicted irradiance
210 close to 0 W/m^2 and greater for values between 40 and 100 W/m^2 .

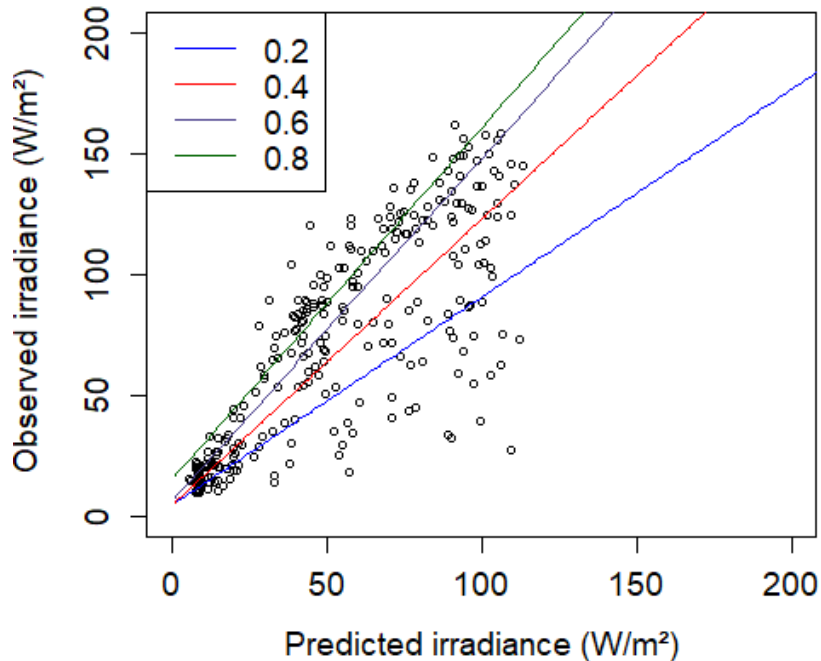


Figure 2: Observed GHI vs. the predicted day-ahead GHI. The lines are the estimates of the quantiles with probability levels of 0.2, 0.4, 0.6 and 0.8. Data are from the training period of Hawaii. Observed and predicted GHI are averaged on the 3-hour window [17h-20h] local time.

211 *2.1.2. The Analog Ensemble (AnEn) technique*

212 The analog ensemble technique is now quite a standard in the energy meteorology fore-
 213 casting community [26, 17]. Similarly to the LQR method, the analog technique is a non-
 214 parametric method that can be used to estimate the predictive CDF of the predictand.

215 Considering a training set of N ordered (sorted by forecasts) pairs of GHI observa-
 216 tions/GHI forecasts $(Y_i, \hat{Y}_i)_{i=1, \dots, N}$, the procedure for determining the forecast CDF is as
 217 follows:

- 218 1. For a new forecast taken from a testing set, calculate its distance from every past
 219 forecast order and find the rank R of the past forecast that is the closest to the new
 220 forecast.
- 221 2. Form an ensemble by selecting the $2\alpha + 1$ past training observations Y_k having their
 222 ranks k inside the interval $[R - \alpha, R + \alpha]$.
3. Compute the predictive CDF at a specific value y of the predictand using the following equation:

$$\hat{F}(y) = P(Y \leq y) = \frac{1}{2\alpha + 1} \sum_{k=1}^{2\alpha+1} H(y - Y_k), \quad (4)$$

223 where Y is the random value related to the predictand (here GHI) and H is the Heaviside
 224 or step function. The effectiveness of the method is strongly dependent on the value of α .
 225 It is proposed here to take $\alpha = 0.02N$. This choice has been motivated by a preliminary
 226 study made on the training period. Appendix C details the selection of the optimal value
 227 of α . Finally, as for the linear quantile regression, note that the GHI forecasts used in the
 228 *AnEn* technique will be given either by the ECMWF control member or the mean of the
 229 ensemble (see Table 2 below).

230 2.1.3. The Nonhomogeneous truncated Gaussian Regression technique (*t_NGR*)

The NGR technique also called in some studies “Ensemble Model Output Statistics” (EMOS) has been introduced by Gneiting et al. [20] for probabilistic forecasting of weather variables. This technique is dedicated to the post-processing of ensemble forecasts produced by an EPS. The NGR technique builds the predictive PDF of the predictand Y from a normal PDF. As such, this kind of model can be termed as a parametric model. The predictive pdf \hat{f} estimated by the NGR method is given by:

$$\hat{f} \sim \mathcal{N}\left(a + \sum_{k=1}^M (b_k m_k), c + dS^2\right), \quad (5)$$

231 where M is the number of members, m_k is the k^{th} member and S^2 is the variance of the
 232 ensemble members distribution. The free parameters a, b_1, \dots, b_M, c and d are determined
 233 with the help of an optimization procedure. In this work, and following Gneiting et al.
 234 [20], these parameters are calculated by minimizing (over a training period) an evaluation
 235 metric for probabilistic forecasts called CRPS (see section 3.2 for details regarding CRPS).
 236 Furthermore, as GHI is a necessarily positive quantity, we propose, in this work, a variant
 237 of the NGR technique namely a truncated version (at 0) of the nonhomogeneous gaussian
 238 regression. In the following, the corresponding model is denoted as *t_NGR*.

239 2.1.4. The Nonhomogeneous Regression of Generalized Extreme Value technique (*NR_GEV*)

240 One can question the choice of a Gaussian distribution in the *t_NGR* technique. Indeed,
 241 the distributions of observations for a fixed forecasting level are actually non-Gaussian. Two
 242 examples for the studied sites are presented in Figure 3.

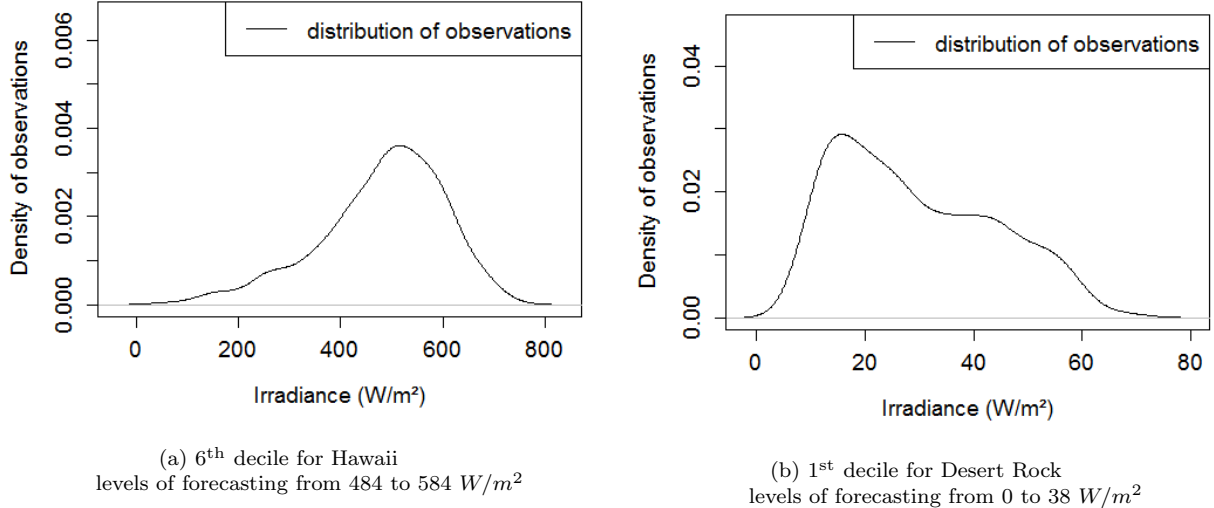


Figure 3: Example of distributions of observations for a fixed forecasting level.

243 On these specific examples, the distributions of observations are clearly non-Gaussian
 244 and the consideration of other types of distributions may improve the skills of the forecast.

245 As pointed out in [21] and [27], other types of parametric distributions can be used
 246 to deal with this issue. Here, a Non homogeneous Regression approach with Generalized
 247 Extreme Value distributions is proposed to estimate the PDF of the predictand Y . The
 248 PDF of a generalized Extreme value distribution for a specific value y of the predictand
 249 GHI is defined as :

$$\hat{f}(y) = \begin{cases} \frac{1}{\sigma} \left[1 + \xi \left(\frac{y-\mu}{\sigma} \right) \right]^{(-\frac{1}{\xi})-1} \exp \left(- \left[1 + \xi \left(\frac{y-\mu}{\sigma} \right) \right]^{-\frac{1}{\xi}} \right) & \xi \neq 0, \\ \frac{1}{\sigma} \exp \left(-\frac{y-\mu}{\sigma} \right) \exp \left[- \exp \left(-\frac{y-\mu}{\sigma} \right) \right] & \xi = 0. \end{cases} \quad (6)$$

250 The parameters μ , σ and ξ are to be determined by optimizing the CRPS over the train-
 251 ing period. We followed the framework of [28] and [29] to set these coefficients. Following
 252 this procedure, the mean μ and the scale parameter σ of the final distributions are deter-
 253 mined by linear regression, and depends only on variables inferred from the EPS. The mean
 254 is a linear combination of the mean of the members and the fraction of members which
 255 predict exactly zero. The scale parameter σ depends on the ‘‘Gini’s mean difference’’ (a
 256 measure of the variability closely related to the spread of the members, see [30] for details).
 257 Note that the shape parameter is taken as a constant. Thus, the minimization of the CRPS
 258 yields the linear coefficients for the mean μ and the scale parameter σ as well as the value of
 259 the shape parameter ξ . Note that the two techniques namely t_NGR discussed above and
 260 NR_GEV discussed here are part of a family of parametric methods named Nonhomoge-
 261 neous Regression (NR).

Site	HAW	DR	SP	PAL	TIR	LAN
Any perturbed member	138	75.3	126.5	97.7	110.7	98.8
Control member	135	72.8	91.9	102.9	100.8	93.2
Mean of the members	129.7	67.9	113.8	81.8	92.6	84.3
Median of the members	133.9	69.4	115.5	84.1	94.7	85.6

Table 1: RMSE (W/m^2) of 4 deterministic forecasts that can be inferred from an EPS: any of the 50 perturbed members of ECMWF ensemble forecast, the control member (unperturbed), the mean of the members and the median of the members. See Table 3 for the signification of the acronyms of the different sites.

262 *2.2. Obtaining probabilistic forecasts from deterministic forecasts (Deterministic-based ap-*
263 *proach)*

264 Some of the techniques presented in section 2.1, namely the Linear Quantile Regression
265 (LQR) and the Analog Ensemble (AnEn) techniques, are capable of generating a probabilistic
266 forecast from a deterministic predictor.

267 In our study, and regarding the deterministic-based approach, the control member of
268 ECMWF-EPS is the predictor variable X of the LQR technique and it will be the forecast
269 used in the AnEn procedure. The corresponding probabilistic models are denoted respec-
270 tively as LQR_c and $AnEn_c$ in the following.

271 *2.3. Obtaining probabilistic forecasts from ensemble forecasts (Ensemble-based approach)*

272 *2.3.1. From the raw output of ECMWF-EPS*

273 Given a raw ensemble forecast of M members $\{m_i\}_{i=1,\dots,M}$, it seems natural to define
274 directly a forecast CDF from this EPS as illustrated in Figure 1. Note that this definition
275 corresponds to the “uniform” definition of a CDF derived from an ensemble” discussed in
276 Lauret et al. [23].

277 *2.3.2. From information extracted from an EPS*

278 An EPS differs from a deterministic forecast by the multiplicity of predictors. In this
279 work, we propose to assess the quality of two variants of probabilistic models built with
280 information extracted from an EPS.

281 The first variant will make use of the mean of the ensemble members of the EPS. The
282 use of the mean of members as a deterministic predictor is justified by Table 1. For all the
283 considered sites depicted in Table 3, Table 1 lists the Root Mean Square Error (RMSE)¹ of
284 different deterministic predictors extracted from an EPS.

285 As shown by Table 1, the mean of all the members turns out to be the best predictor for
286 deterministic forecasting. Hence, to quantify the improvement brought by the first moment
287 estimation (i.e. the mean), two models denoted by LQR_m and $AnEn_m$ based respectively
288 on the LQR and AnEn techniques will be evaluated.

¹RMSE is a common metric used to assess the accuracy of deterministic forecasts [31]

Approach	Deterministic-based		Ensemble-based			
Predictors	Control member		Mean of members		Mean and spread of members	
Technique	AnEn	LQR	AnEn	LQR	LQR	NR
Model Abbreviation	$AnEn_c$	LQR_c	$AnEn_m$	LQR_m	LQR_s	t_NGR NR_GEV

Table 2: Summary of all considered forecasting models with AnEn: Analog Ensemble, LQR: Linear Quantile Regression, NR: Nonhomogeneous Regression

289 The second variant will include, in addition to the mean of the members, the spread (i.e.
290 the variance) of the members of the EPS. The t_NGR and the NR_GEV models described
291 in sections 2.1.3 and 2.1.4 use the first and second moment of the EPS distribution to build
292 the predictive distributions. Furthermore, we also propose to use the LQR technique with
293 a vector X of predictors given by

$$X = [\mu, S^2], \quad (7)$$

294 where μ represents the mean of members and S^2 the variance of the ensemble. This method
295 will be referred in this study as LQR_s . Finally, Table 2 summarizes the different probabilistic
296 models that will be evaluated in this study.

297 3. Verification of the probabilistic forecasts

298 In this section, we detail some of the verification tools proposed by Lauret et al. [23]
299 that will be applied to assess the quality of GHI probabilistic forecasts. Following this work,
300 we will rely on a quantitative score namely the continuous ranked probability score (CRPS)
301 and its related skill score (CRPSS) to rank objectively the different methods. Moreover, and
302 based on the recommendations of [23], we will provide the decomposition of the CRPS into
303 the main attributes that affect the quality of the forecasts. In addition to this decomposition,
304 it is worth noting that we will propose in this work a new way to have detailed insight into
305 the performance of the methods. This new methodology is based on the contribution of the
306 moments (mean, variance, etc.) of the forecast distribution to the CRPS (see section 3.3
307 below).

308 3.1. Attributes for a skillful probabilistic model

309 We recall here briefly the two main attributes that characterize the quality of the prob-
310 abilistic models namely reliability and resolution [32, 33]. Reliability or calibration evalu-
311 ates the statistical consistency between the forecasts and the observations. In the case of
312 a continuous variable like GHI, a high reliability is obtained if predictive distributions and
313 distributions of observations agree. Resolution refers to the ability of the probabilistic model
314 to discriminate among different forecast situations. More precisely, the more distinct the
315 observed frequency distributions for various forecast situations are from the full climatolog-
316 ical distribution, the more resolution the forecast model has. A high quality probabilistic
317 model should issue reliable forecasts with high resolution. In other words, high reliability is

318 a necessary but not a sufficient condition for a high quality probabilistic forecast. The fore-
 319 cast should also exhibit high resolution. For instance, climatological forecasts are perfectly
 320 reliable but exhibit no resolution.

321 3.2. CRPS

322 In the verification framework proposed by Lauret et al. [23], the authors recommend the
 323 computation of a score like the Continuous Ranked Probability Score (CRPS) to evaluate
 324 the overall quality of the probabilistic models. We recall here the definition of the CRPS.

325 3.2.1. Definition

The CRPS measures the difference between the predicted and observed cumulative dis-
 tributions functions (CDF) [34]. The CRPS reads as

$$CRPS = \frac{1}{N} \sum_{i=1}^N \int_{-\infty}^{+\infty} \left[\hat{F}_{fcst}^i(y) - F_{y_{obs}}^i(y) \right]^2 dy, \quad (8)$$

326 where $\hat{F}_{fcst}(y)$ is the predictive CDF of the predictand Y (here GHI) and $F_{y_{obs}}(y)$ is a
 327 cumulative-probability step function that jumps from 0 to 1 at the point where the value
 328 of the predictand y equals the observation y_{obs} (i.e. $F_{y_{obs}}(y) = 1_{\{y \geq y_{obs}\}}$). The squared
 329 difference between the two CDFs is averaged over the N forecast/observation pairs. The
 330 CRPS score rewards concentration of probability around the step function located at the
 331 observed value [32]. In other words, the CRPS penalizes lack of resolution of the predictive
 332 distributions as well as biased forecasts. Note that the CRPS is negatively oriented (smaller
 333 values are better) and it has the same dimension as the forecasted variable. CRPS is a
 334 proper score meaning that it obtains the best expected value when the forecast distribution
 335 is equal to the true distribution of probability of the observation. Besides, using proper
 336 scoring rules allows the decomposition of the score into the two important attributes of the
 337 quality of a forecasting probabilistic model namely resolution and reliability. This permits
 338 to understand more precisely the characteristics of the quality of the forecast.

339 3.2.2. CRPS Skill Score

340 In a similar manner, skill scores are used to assess the forecast skill of deterministic
 341 forecasts [35], Pedro et al. [36] used the CRPS Skill Score (CRPSS) to gauge the quality of
 342 their probabilistic forecasting models against a reference method. The CRPSS metric (in
 343 %) reads as

$$CRPSS = 100 \times \left(1 - \frac{CRPS_m}{CRPS_r} \right), \quad (9)$$

344 where $CRPS_r$ denotes the CRPS of the reference method and $CRPS_m$ refers to the CRPS
 345 of the model under evaluation (see Table 2). A negative value of CRPSS indicates that
 346 the probabilistic method fails to outperform the reference model while a positive value of
 347 CRPSS means that the forecasting method improves on the reference model. Further, the
 348 higher the CRPSS, the better the improvement.

349 In this work, and following the recommendations of Doubleday et al. [37], the raw output
 350 of the ECMWF-EPS serves as the reference benchmark model.

351 3.2.3. Decomposition of the CRPS

The decomposition of the CRPS is given by :

$$CRPS = REL - RES + UNC, \quad (10)$$

352 where REL, RES and UNC are respectively the reliability part, the resolution part and the
 353 uncertainty part of the CRPS. The interested reader is referred to [23] for details regarding
 354 the computation of the different components of the CRPS.

355 In addition to reliability and resolution, the uncertainty term accounts for the variability
 356 of the observations. It is an indication of the difficulty to forecast the variable of interest and
 357 cannot be modified by the forecasting model. It is also worth noting that the uncertainty part
 358 UNC corresponds to the score of the climatology. For scores like CRPS that are negatively
 359 oriented, the goal of a forecasting model is to minimize (resp. maximize) as much as possible
 360 the reliability term (resp. the resolution term). In fact, a forecasting model with a high
 361 resolution term means that the model has captured the maximum of the variability present
 362 in the data (which variability is measured by the uncertainty term).

363 3.3. Contributions of the statistical moments of the forecast distribution to the CRPS

364 In this study, a new methodology for a better understanding of the skills of a probabilistic
 365 forecast in relation with the CRPS score is developed. The main idea is to assess separately
 366 the contribution of the statistical moments (mean, variance, etc.) of the predictive distribu-
 367 tions to the CRPS and consequently to the quality of a probabilistic forecasting model. The
 368 principle of the method is to create two virtual forecasts which show the contribution of the
 369 statistical moments of the actual forecast to the CRPS. Let us illustrate the methodology
 370 with 3 forecast PDFs depicted in Figure 4. f represents the actual forecast PDF and f_{m1}
 371 and f_{m2} the associated virtual PDF forecasts.

The first virtual forecast f_{m1} is derived from the first moment (mean) of the actual
 forecast f . Let m_1 be the first moment of f and δ the Dirac distribution (corresponding to
 the dotted vertical line in Figure 4), the PDF of f_{m1} is thereby defined by:

$$f_{m1}(y) \equiv \delta(y - m_1). \quad (11)$$

372 Note that this definition implies that the second, third and further moments of f_{m1} are equal
 373 to 0.

The second virtual forecast f_{m2} is given by a Gaussian distribution with first and second
 moments equal to those of f . Let m_2 be the second moment of f , f_{m2} is defined as:

$$f_{m2} \sim \mathcal{N}(m1, m2). \quad (12)$$

374 Being a Gaussian distribution, the third, fourth and further moments of f_{m2} are equal to 0.

The contribution of the statistical moments of the distribution to the CRPS is computed
 as follows. First, the CRPS of each forecast namely $CRPS_f$, $CRPS_{f_{m1}}$ and $CRPS_{f_{m2}}$

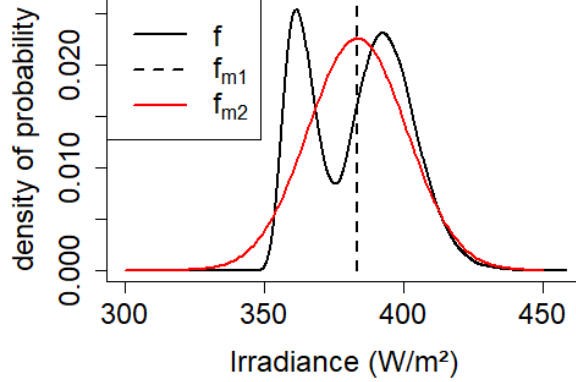


Figure 4: Illustration of the virtual forecasts f_{m1} and f_{m2} related to the forecast PDF f

are averaged over the N forecast/observation pairs. This leads to the corresponding values $CRPS$, $CRPS_{m1}$ and $CRPS_{m2}$. Second, the difference $G_2 = CRPS_{m1} - CRPS_{m2}$ and $G_+ = CRPS_{m2} - CRPS$ are calculated. Note that one can therefore rewrite the CRPS as:

$$CRPS = CRPS_{m1} - G_2 - G_+. \quad (13)$$

375 Note that the $CRPS_{m1}$ of the deterministic forecast f_{m1} is actually its Mean Absolute
 376 Error (MAE)² (see [34] for details).

377 G_2 is the measure of the gain in CRPS or equivalently in forecast quality that results
 378 from the additional information brought by the second moment of the distribution. G_+
 379 represents the gain resulting from the other statistical moments. G_2 is assumed to be
 380 positive. If it is found negative, then the probabilistic forecast has no added value compared
 381 to a deterministic forecast. Indeed, the CRPS of the probabilistic forecast would be higher
 382 than the CRPS of the deterministic one ($CRPS_{m1}$, which is the MAE), thus denoting a loss
 383 of quality of the probabilistic forecast. On the other hand, G_+ is generally positive. It can
 384 be null or negative if the forecast distribution obtains a higher CRPS score than a Gaussian
 385 distribution defined by $\mathcal{N}(m1, m2)$. This would indicate that the forecast distribution is less
 386 suitable than a Gaussian distribution.

387 In section 5.3 below, we propose to present this diagnostic tool under the form of a
 388 bar-plot, where $CRPS$, G_+ and G_2 are stacked in this order. G_2 is denoted by the pink
 389 part of the bar, G_+ by the green part and $CRPS$ by the blue part. Note that a black line
 390 on the top of the blue part is used to better highlight the value of the CRPS and a dotted
 391 black line indicates $CRPS_{m1}$ (see Figure 6). In the following, we refer to this diagnostic
 392 tool based on the contribution of the moments of the forecast distributions to the CRPS as
 393 “MC-CRPS”.

²Similarly to RMSE, MAE is also a common metric used to assess the accuracy of deterministic forecasts.

394 4. Case studies

395 Six sites are chosen to test the selected models. The first one, Desert Rock, which is part
396 of the SURFRAD network, is located in an arid area. It experiences a high occurrence of
397 clear skies and consequently a very low variability. Two other sites, the airport of Hawaii,
398 where the NREL set up a radiometric network, and Saint-Pierre, which is located on the
399 coastal part of the island La Réunion, are insular sites. Both present a high yearly solar
400 irradiation but also an important variability due to frequent partly cloudy skies. These
401 differences between the two types of sites will permit testing the models under different sky
402 conditions. For an extensive study on the multiple factors that impact the climatology and
403 sky conditions in the specific case of Saint-Pierre and La Réunion, see Badosa et al. [38] or
404 Kalecinski [39].

405 As the aforementioned sites exhibit a similar level of irradiation, three other BSRN sites
406 namely Palaiseau, Tiruvallur and Langley are also considered to test our methodology. The
407 six chosen sites experience different levels of annual solar irradiation and of sky conditions.
408 Thus, this set of sites is representative of the various climates around the world. The main
409 characteristics of these six sites are given in Table 3. The solar variability, presented in the
410 last line of Table 3, is defined as the standard deviation of the changes in the clear sky index
411 [40].

412 4.1. Measurements

413 The measured data used in this work are global horizontal irradiance (GHI) time series
414 recorded at the six considered sites. These datasets have been prepared for previous works
415 related to the development and the benchmarking of probabilistic solar forecasts [41, 42].
416 They correspond to two years of data divided in a training set (the first year) and test set
417 (the second year). As the ensemble forecasts used here are provided with a 3-hour time step,
418 the recorded time series, initially formatted with a 1-hour granularity, were averaged with
419 a 3-hour time step. A quality check and several test were performed on the recorded GHI
420 time series. The results are given in Appendix A.

	Desert Rock (USA)	Hawaii (USA)	Saint-Pierre (Reunion)
Acronym	DR	HAW	SP
Provider	SURFRAD	NREL	PIMENT
Position	36.6N, 119.0W	21.3N, 158.1W	21.3S, 55.5E
Elevation (m)	1007	11	75
Climate type	Desert	Insular tropic	Insular tropic
Years of record	2012 - 2013	2010-2011	2012 - 2013
Annual solar irradiation (MWh/m^2)	2.105	1.969	2.053
Solar variability 1-h ($\sigma\Delta kt_{1hour}^*$)	0.146	0.209	0.241
	Palaiseau (France)	Tiruvallur (India)	Langley (USA)
Acronym	PAL	TIR	LAN
Provider	BSRN	BSRN	BSRN
Position	48.7N, 2.2E	13.1N, 80.0E	37.1N, 76.4W.
Elevation (m)	156	36	3
Climate type	Mild oceanic	Monsoon	Humid
Years of record	2016-2017	2018-2019	2015-2016
Annual solar irradiation (MWh/m^2)	1.172	1.835	1.685
Solar variability 1-h ($\sigma\Delta kt_{1hour}^*$)	0.281	0.190	0.186

Table 3: Main characteristics of time series of recorded global horizontal irradiance (GHI) used to test the models.

421 4.2. Forecasts

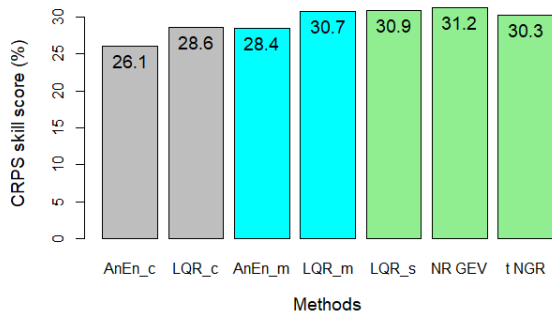
422 As mentioned above, the initial day-ahead ensemble forecasts, covering the same period
423 as the measurements, are provided by the European Centre of Medium-Range Weather
424 Forecasts (ECMWF). The EPS is released by ECMWF at 12:00 for the 72 next hours with
425 a 3-hours timestep which allows it to be used for day-ahead scheduling or trading purposes.

426 5. Results

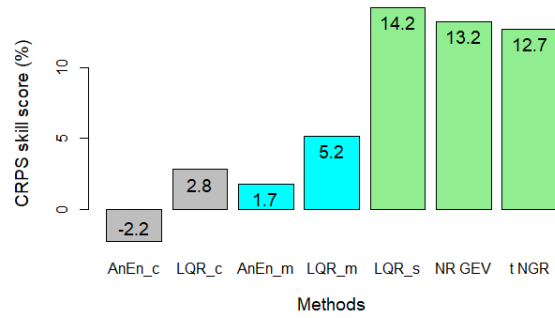
427 Based on the verification framework proposed by Lauret et al. [23], the overall perfor-
428 mance of the different probabilistic methods is measured by the CRPS and the CRPSS.
429 Detailed insight in the quality of the models is obtained through the decomposition of the
430 CRPS and the new ‘‘MC-CRPS’’ method. Note that this section is dedicated to the pre-
431 sentation of the main results of the study. The next section will be devoted to an in-depth
432 discussion related to the pros and cons of each approach and the added-value brought by
433 the MC-CRPS methodology.

434 5.1. Overall performance of the methods

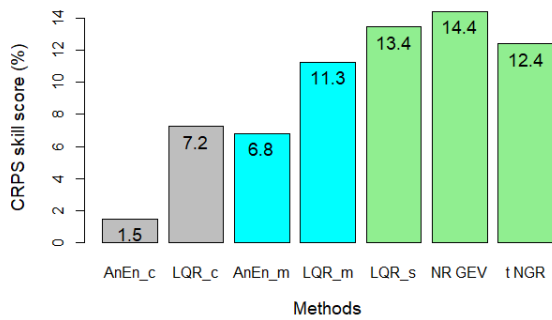
435 Table 4 lists the CRPS obtained by the different methods. However, in order to better
436 highlight the relative merits of each approach, Figure 5 shows the CRPS skill scores of all



(a) Hawaii



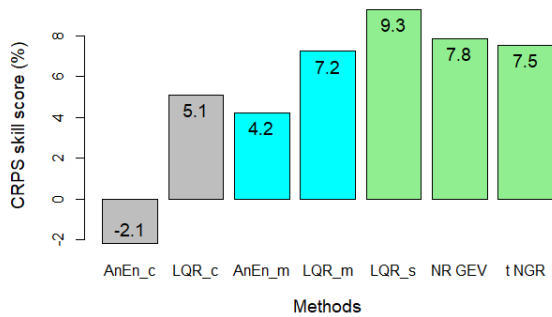
(b) Desert Rock



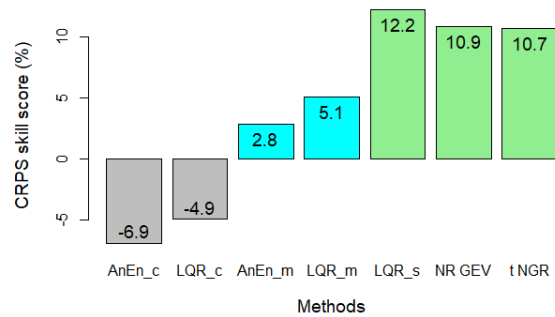
(c) Saint-Pierre



(d) Palaiseau



(e) Tiruvallur



(f) Langley

Figure 5: CRPS Skill Score of all models for the six considered sites. Grey : deterministic-based approach, Cyan : ensemble-based approach using the mean of the members, Green : ensemble-based approach using mean and standard deviation of the members.

437 the forecasting models. Let us recall that positive values of skill scores mean that the model
438 outperforms the reference model (here the raw ECMWF-EPS) while negative values reveal
439 that the quality of the evaluated model is worse than the reference one.

440 As shown by Figure 5, regardless the site under study, the highest CRPS skill scores are
441 obtained by the ensemble-based approach (represented by the cyan and green bars). Con-
442 versely, except the case of Hawaii, the deterministic-based approach (grey bars) yields lower
443 or even negative skill scores. These negative CRPS values indicate that the deterministic-
444 based models do not always achieve to increase the quality of the raw ensemble forecasts
445 (see for example Palaiseau and Langley).

446 A deeper look into the performance of the ensemble-based approach shows that models
447 using the mean and the standard deviation of the ensemble members (green bars) exhibit
448 a better forecast skill than models using only the mean of the members (cyan bars) albeit
449 the improvement is less pronounced for Hawaii. Overall, the model with the highest skill
450 score appears to be either LQR_s or NR_GEV . Regarding the latter, it may suggest that
451 a judicious choice of the underlying PDF (see Equation 6) used by a calibration technique
452 like Nonhomogenous Regression (NR) can further improve the quality of the probabilistic
453 forecasts.

454 Finally, in order to quantify the relative improvement provided by the ensemble-based
455 approach over the deterministic-based approach, we calculate the gain in CRPS based on
456 the CRPS values of the best performer of each approach. It appears that the level of
457 improvement is very dependent on the studied site. It is moderate for Hawaii and Tiruvallur
458 (4%), becomes larger for Saint-Pierre (approximately 8%) and quite significant for Desert
459 Rock (approximately 12%), Langley and Palaiseau (approximately 16%).

460 5.2. Detailed insight through the decomposition of the CRPS

461 Table 4 also provides the decomposition of the CRPS into reliability and resolution of
462 the different forecasting methods. As mentioned previously, a forecast should exhibit a small
463 reliability term and a large resolution term. It is worth mentioning first that all models sig-
464 nificantly improves the reliability component of the raw EPS forecasts and that the level of
465 improvement strongly depends on the reliability of the initial raw ensemble. Second, it can
466 be noted that the reliability of all calibrated forecasts is fairly comparable. In addition, re-
467 gardless the site, it appears that, overall, the ensemble-based approach does not significantly
468 improve reliability compared to the deterministic-based approach. Looking in more details,
469 models based on the $AnEn$ technique often appears to generate the most reliable forecasts
470 while the t_NGR model generally provides the less reliable forecasts. Also, in the case of
471 Non homogeneous calibration technique, GEV distributions seem to be more suitable than
472 Gaussian distributions, since NR_GEV is slightly more reliable than the t_NGR model.

473 Regarding the resolution component, it must be noted first that the deterministic-based
474 approach fails to improve the resolution of the raw Ensemble. Conversely, resolution in-
475 creases with the ensemble-based approach, and particularly when the spread of EPS mem-
476 bers is taken as as input of the models i.e. case of the LQR_s, t_NGR and NR_GEV models.
477 Finally, one can state that the decomposition of the CRPS given in Table 4 reveals that

	Site	HAW	DR	SP	PAL	TIR	LAN
CRPS (W/m^2)	raw Ensemble	67.7	29.4	59.4	38.6	46.8	40.0
	<i>AnEn_c</i>	50.1	30.1	58.5	44.0	47.8	42.8
	<i>LQR_c</i>	48.4	28.6	55.1	43.3	44.4	42.0
	<i>AnEn_m</i>	48.5	28.9	55.3	38.4	44.9	38.9
	<i>LQR_m</i>	46.9	27.9	52.7	38.6	43.4	38.0
	<i>LQR_s</i>	46.8	25.2	51.4	36.2	42.5	35.2
	<i>t_NGR</i>	47.2	25.7	52.0	36.2	43.3	35.8
	<i>NR_GEV</i>	46.6	25.5	50.8	36.2	43.2	35.7
Reliability (W/m^2)	raw Ensemble	23.2	8.4	13.4	7.5	11.5	8.2
	<i>AnEn_c</i>	4.2	4.8	6.6	4.9	7.2	4.8
	<i>LQR_c</i>	4.4	5.3	7.1	5.4	6.7	5.3
	<i>AnEn_m</i>	4.1	4.7	6.2	4.9	7.9	4.5
	<i>LQR_m</i>	4.4	5.7	7.0	5.7	8.2	5.0
	<i>LQR_s</i>	4.5	5.9	7.6	5.3	8.2	5.4
	<i>t_NGR</i>	4.7	6.5	8.4	5.4	8.0	5.7
	<i>NR_GEV</i>	4.1	6.2	7.2	5.4	7.8	5.8
Resolution (W/m^2)	raw Ensemble	113.3	154.0	126.7	95.4	125.7	122.5
	<i>AnEn_c</i>	111.9	149.7	120.8	87.4	120.4	116.4
	<i>LQR_c</i>	113.9	151.7	124.7	88.6	123.3	117.7
	<i>AnEn_m</i>	113.4	150.8	123.5	93.0	124.0	120.0
	<i>LQR_m</i>	115.3	152.8	127.0	93.6	125.8	121.4
	<i>LQR_s</i>	115.5	155.6	128.9	95.6	126.8	124.7
	<i>t_NGR</i>	115.3	155.7	129.0	95.8	125.8	124.3
	<i>NR_GEV</i>	115.3	155.6	129.1	95.6	125.7	124.5
Uncertainty (W/m^2)	All Models	157.8	175.0	172.7	126.5	161.0	154.4

Table 4: CRPS and its components reliability, resolution and uncertainty of all considered models for the 6 sites. Cyan : deterministic-based approach, Green : ensemble-based approach. Red values indicate the worst CRPSs while the black bold ones show the best CRPSs.

478 the difference in quality between the two approaches is mainly explained by the resolution
 479 component, whereas reliability is fairly comparable.

480 *5.3. Detailed insight through the CRPS Moments-Contributions*

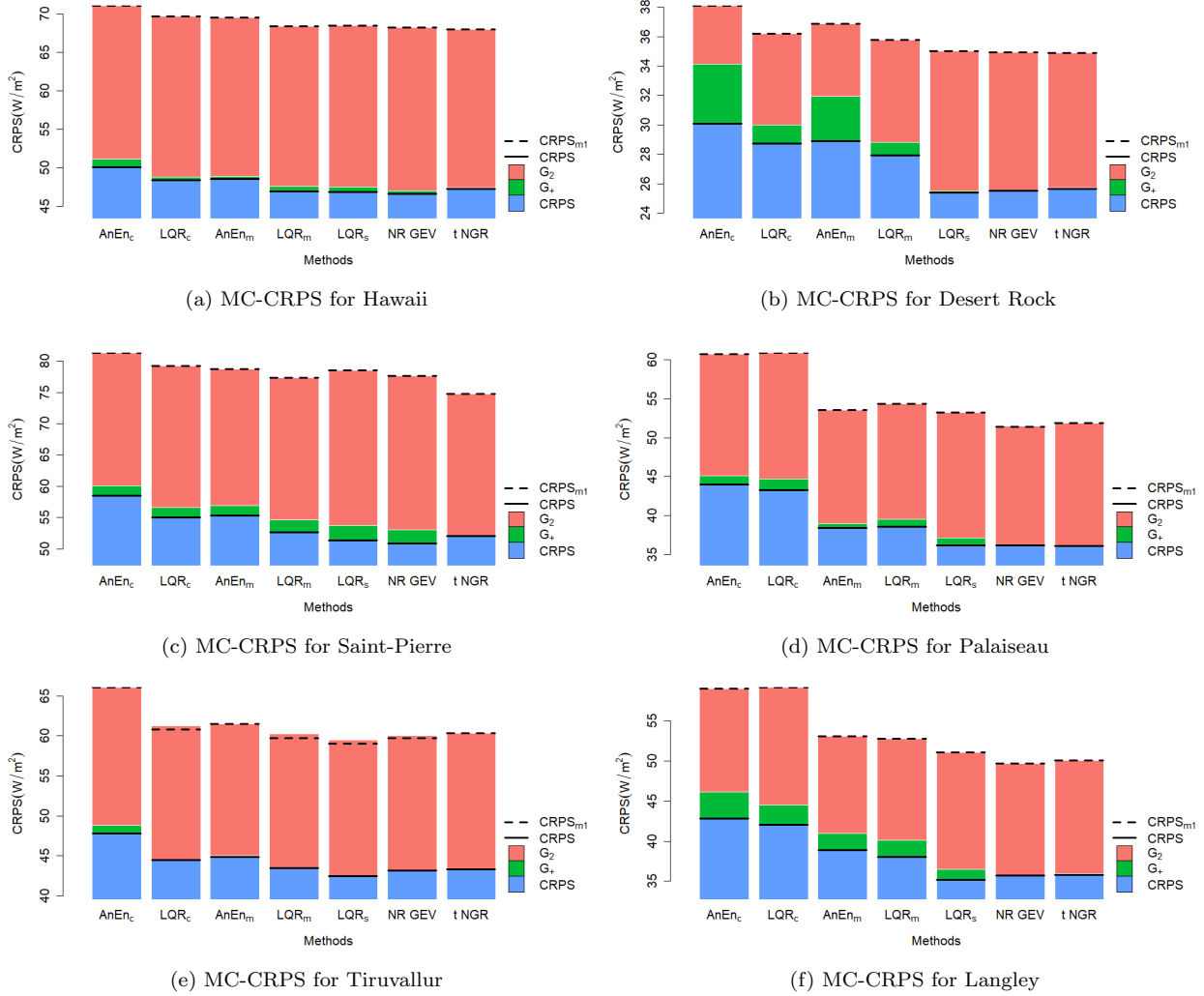


Figure 6: MC-CRPS of the six sites and all forecasting models. A black line is used to better highlight the value of the CRPS and a dotted black line indicates the value of $CRPS_{m1}$.

481 Figure 6 shows the results of the MC-CRPS introduced in section 3.3. As seen, the
 482 final CRPS values, of the forecasting models occur to be dependent on their respective
 483 $CRPS_{m1}$ values. In particular, models from the ensemble-based approach appear to have
 484 best $CRPS_{m1}$ than models from the deterministic-based approach (see for instance the case
 485 of Langley). This means that the aggregation of members improves the estimation of the first
 486 moment. Among the ensemble-based models, except for the cases of Hawaii and Tiruvallur,
 487 the superiority of the LQR_s , NR_GEV and $tNGR$ models using the mean and standard

488 deviation of the ensemble members can be mainly explained by a greater contribution of
489 G_2 . Thus the spread of EPS members is effective and improves more importantly G_2 than
490 $CRPS_{m1}$. Further, the best performer among the three aforementioned models is finally
491 determined by G_+ . This highlights the importance of the choice of the distribution in the
492 non homogenous regression calibration framework.

493 For example, overall, NR_{GEV} performs better than the t_{NGR} model because of G_+ .
494 Let us stress that the choice of strictly truncated Gaussian distributions in the implemen-
495 tation of a NGR technique forces G_+ to be very close to 0 in the MC-CRPS. Hence, the
496 benefits of GEV distributions compared to Gaussian distributions are highlighted by the
497 MC-CRPS method.

498 6. Discussion

499 In this section, we try to give more clues regarding the merits of each proposed approach.
500 Also, a discussion related to the advantages brought by the MC-CRPS is proposed.

501 6.1. Deterministic-based approach versus ensemble-based approach

502 Let us recall that the deterministic-based approach uses a unique deterministic predictor
503 while the ensemble-based approach makes use of the information conveyed by the ensemble.
504 Therefore, the main weakness of the deterministic-based approach is the lack of information
505 feeding the models. Since the distribution needs to be completely determined from one single
506 deterministic predictor, the spread and the possible skewness and kurtosis of the forecasting
507 distribution need to be only inferred from this single predictor. Conversely, the benefits
508 gained from the multiplicity of predictors provided by the ensemble-based approach need to
509 be significant to justify the computation of the EPS. Two types of benefits can be discussed.

510 First, the aggregation of predictors leads to a better estimation of the first moment.
511 This is visible in Figure 6 where models issued from the ensemble-based approach get better
512 $CRPS_{m1}$ than models from the deterministic-based approach. It is clear that a gain in the
513 estimation of the first moment can be obtained by the substitution of the control member
514 by the mean of all members.

515 Second, regarding the determination of the second moment, the uncertainty is already
516 carried by the level of forecasting of the mean of the EPS members. These variables are
517 dependent, as shown in Appendix B (the standard deviations of the observations clearly
518 depends on the level of forecasting). Hence, using the spread of the members of EPS as
519 input of the forecasting models can only be justified if it brings an extra-information on the
520 uncertainty. It is assumed that the spread of the members is higher if the uncertainty is so.
521 Indeed it indicates if slight errors in the initial conditions could lead to great differences in
522 the final state of the atmosphere.

523 Thus, it appears necessary to investigate on the quantity of information actually provided
524 by the spread of the members. In order to do this, the correlation between the standard
525 deviation of the observations and the spread of the members has been studied. This has been
526 made for a fixed level of forecasting, in order to remove the dependency between uncertainty
527 and level of forecasting. Then an average over all levels of forecasting has been calculated

528 to produce Figure 7. This kind of plot is of great utility to know the added value of the
 529 standard deviation of the EPS forecast members. If the dependence between the spread of
 530 the members and the uncertainty of the forecast for a fixed level of forecasting is strong,
 531 then a large improvement can be expected for calibration models using the spread of the
 532 members as an input, compared to simpler models.

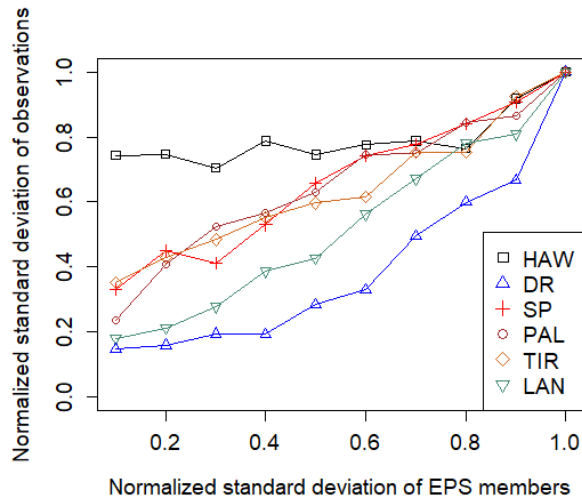


Figure 7: Standard deviation of observations vs. standard deviation of the EPS members (raw ECMWF ensembles). Normalization of the standard deviation has been done by dividing the standard deviations by the maximum of the standard deviation for each site.

533 As shown by Figure 7, the amount of new information given by the spread of the members
 534 is very dependent on the studied site. When for Hawaii, the correlation between the standard
 535 deviation of the observations and the spread of the members is almost null, it is quite
 536 significant for the other sites and especially for Langley and Desert Rock. A link can be
 537 established between this finding and Figure 5 which shows that the success of taking into
 538 account the spread of members in the forecasting models depends on the site. It is clearly
 539 less valuable in Hawaii than in other sites, and it is particularly successful in Desert
 540 Rock and Langley. It is also consistent with Figure 6 where G_2 is significantly higher in Desert
 541 Rock for LQR_s , t_NGR and NR_GEV models.

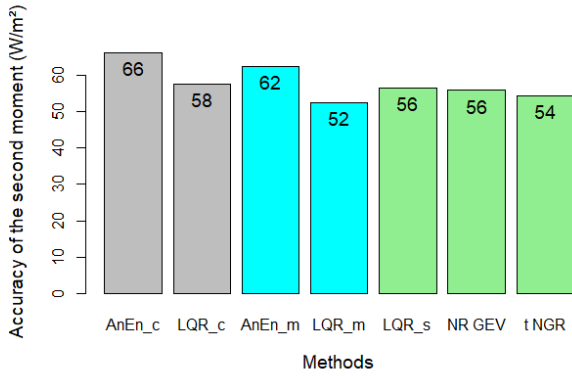
542 6.2. Discussion related to CRPS Moments-Contributions

543 In order to consolidate the results obtained in Figure 6, a complete analysis of the
 544 statistical moments of the probability distributions produced by the forecasting methods
 545 has been conducted. This kind of study is traditionally done to assess the strengths and
 546 weaknesses of a forecasting model. Although the deterministic measure of a statistical
 547 moment is not a proper scoring rule, it is of great interest to use it to understand the
 548 behaviour of the forecasting models.

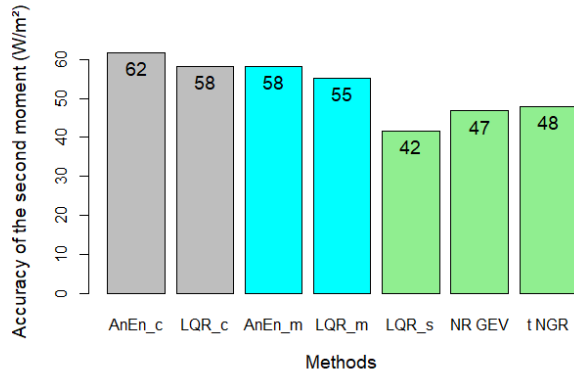
549 First, an evaluation of the accuracy of the first moment has been conducted. A good
 550 forecasting model should have the ability to give a mean value of the forecasting distributions

551 as close as possible to the mean of the observation values. A measure of this ability can
552 be obtained by calculating the Root Mean Square Error (RMSE) or Mean Absolute Error
553 (MAE) of the mean of the forecasting distributions. In this study, the MAE has been
554 chosen as it is exactly the definition of $CRPS_{m1}$ introduced in section 3.3 (see [34] for
555 details). Figure 6 gives therefore the results related to the accuracy of the first moment of
556 the distributions.

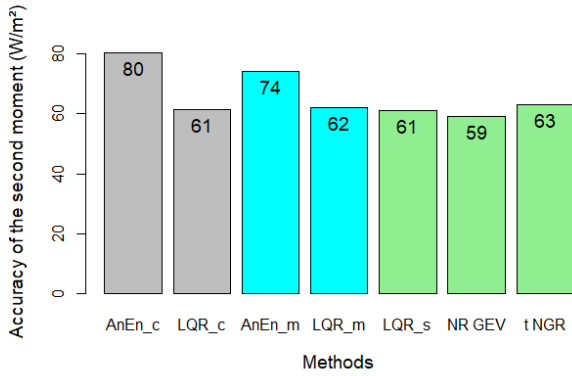
557 Second, a probabilistic forecast also provides an estimation on the level of uncertainty,
558 which is reflected by the spread of the forecasting distribution (i.e. the second statistical
559 moment). Some works have been specifically dedicated to the assessment of the accuracy
560 of the spread of the predictive distributions. Among others, one can cite the studies related
561 to the spread-skill relationship (see [43] or [44]). These works are guided by the idea that
562 the variance of a probabilistic forecast should be larger if the uncertainty of the forecast is
563 so. Fortin et al. [45] proposed a criterion for the evaluation of the accuracy of the second
564 moment of the distributions. This criterion is based on the fact that statistical consistency
565 requires that the spread of the forecasting distributions should be equal to the RMSE of the
566 mean of the forecast. Following [45], spread is calculated as the square root of the mean
567 of the variances of the forecasting distributions. The accuracy of the second moment is
568 therefore measured by calculating the RMSE of the differences between spread and RMSE
569 of the mean of the distributions (i.e. $RMSE_M$). Figure 8 plots the RMSE of the difference
570 ($spread - RMSE_M$), computed over the evaluation period.



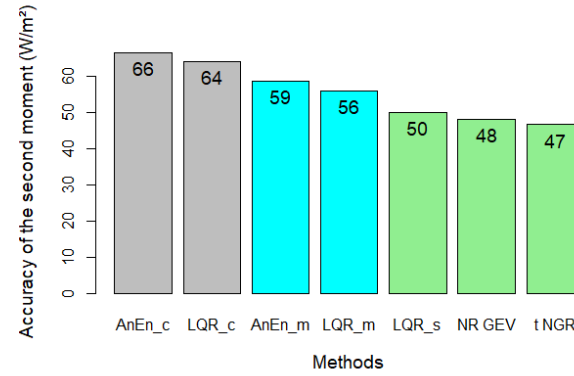
(a) Hawaii



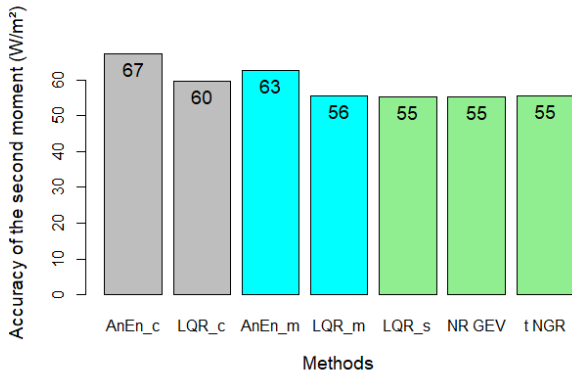
(b) Desert Rock



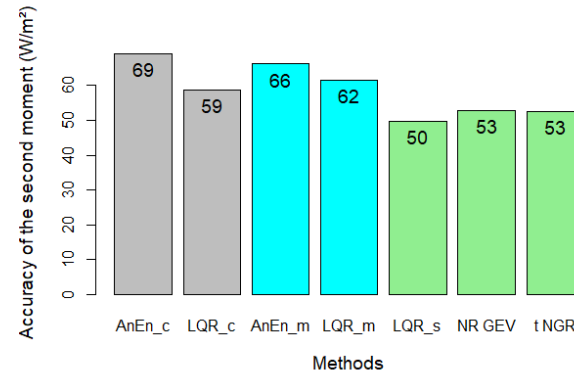
(c) Saint-Pierre



(d) Palaiseau



(e) Tiruvallur



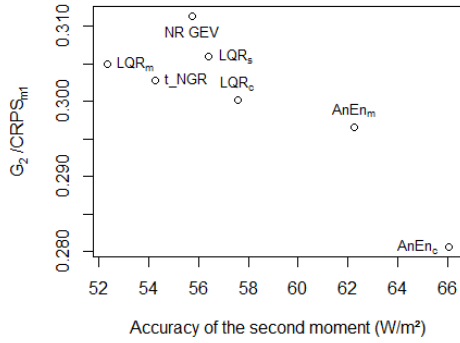
(f) Langley

Figure 8: Accuracy of the second moment for the six studied sites and all forecasting models

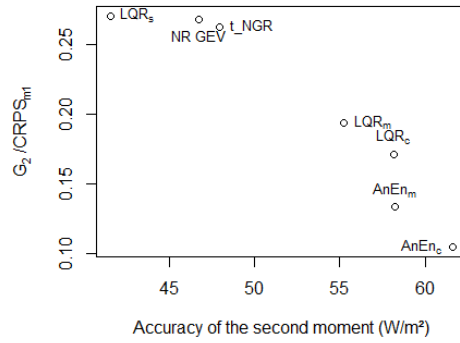
571 Conversely to the first moment, the accuracy of the second moment gradually improves
 572 when the information taken by the forecasting model is more complete. Using the mean
 573 of members instead of the control member increases the second moment accuracy. Taking
 574 into account the spread of the EPS improves further the accuracy by approximately the

575 same extent (except for Hawaii, for the reasons discussed in section 6.1). Nevertheless,
576 this improvement depends on the site. As shown by Figure 8, the accuracy of the second
577 moment for Hawaii is almost equal for each model. It is consistent with the results depicted
578 in Figure 7, showing that the information of the second moment of the EPS distribution in
579 Langley and Desert Rock is the most valuable , as opposed to the information of Hawaii
580 EPS distribution.

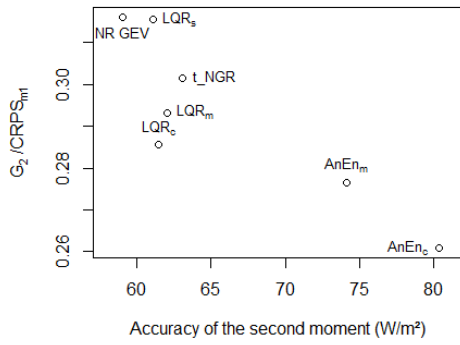
581 The accuracy of the second moment can be linked to the gain G_2 introduced in the MC-
582 CRPS section (see section 3.3). The correlation between these two values is highlighted in
583 Figure 9, which shows the ratio $G_2/CRPS_{m1}$ versus the accuracy of the second moment.



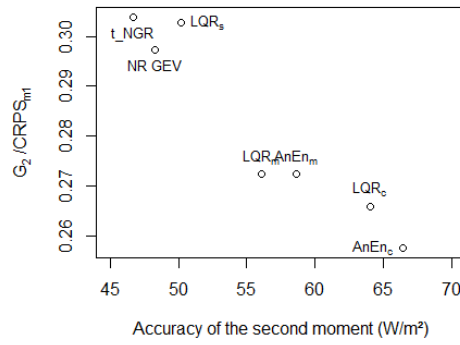
(a) Hawaii



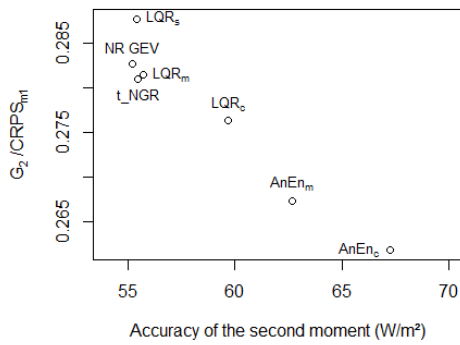
(b) Desert Rock



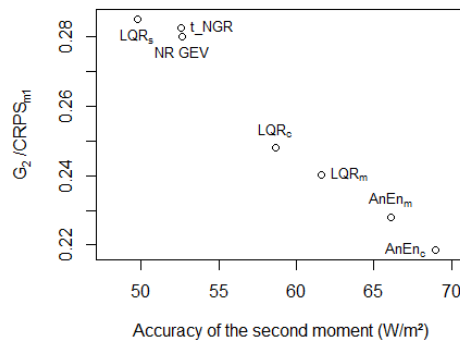
(c) Saint-Pierre



(d) Palaiseau



(e) Tiruvallur



(f) Langley

Figure 9: Link between G_2 and the accuracy of the second moment.

584 To sum up, the great advantage of the MC-CRPS is to reconcile the score of a proba-
 585 bilistic forecasting model and the explanation of its performance by examining the accuracy
 586 of the moment-based distributions.

587 Moreover, the link between the calibration of the moments and the score is highlighted,
588 because the contribution of the accuracy of the moments to the score is quantified. Here,
589 in the proposed new diagnostic tool MC-CRPS, the accuracy of the statistical moments of
590 the forecasting distributions is quantified by the proper score itself. This diagnostic tool
591 is complementary of the decomposition discussed in section 3.2.3, i.e. the reliability and
592 resolution of f_{m1} and f_{m2} can also be computed and studied. The MC-CRPS diagnostic
593 tool also highlights the benefits of probabilistic forecasting, as the comparison between
594 $CRPS_{m1}$ and $CRPS$ provides a measure of the quality difference between deterministic and
595 probabilistic forecasting.

596 7. Conclusions

597 Based on the two types of forecasts i.e deterministic or ensemble forecast (denoted by the
598 term EPS for ensemble prediction system) issued by the meteorological centre ECWMF, two
599 approaches for generating day-ahead solar irradiance probabilistic forecasts were proposed.
600 The first approach creates probabilistic forecasts from the deterministic day-ahead GHI
601 predictor while the second one generates probabilistic forecasts from the calibration of the
602 EPS or from information inferred from the EPS.

603 The goal of this work was to quantify the possible added-value of the EPS on the quality
604 of the forecasts. Six sites experiencing different sky conditions were chosen for the appraisal
605 of the different probabilistic models. Quality of the different probabilistic models have been
606 evaluated with common diagnostic tools such as the CRPS and its decomposition. A new
607 diagnostic tool called MC-CRPS has also been introduced. It consists in the measure of the
608 contribution of each statistical moment of the forecasting distributions to the CRPS.

609 Overall, models adopting the ensemble-based approach have been found to issue proba-
610 bilistic forecasts with better quality than the ones based on the deterministic-based approach.
611 The gain in quality, based on the CRPS metric, ranges from 4 % up to 16 %.

612 One other important contribution of this work is the new diagnostic tool related to the
613 CRPS score based on the moments of the ensemble distribution called MC-CRPS. This
614 MC-CRPS tool allowed to identify two characteristics of EPS that have an impact on the
615 quality of probabilistic forecasts. First, the aggregation of deterministic predictors of the
616 ensemble leads to an improvement of the estimation of the first moment and thus, raises the
617 overall quality of a probabilistic forecast. Second, the spread of the EPS members turns to
618 be a good predictor that permits to enhance the estimation of the second moment of the
619 forecasting distributions. Finally, in terms of forecast quality, it can be concluded that using
620 an EPS (which requires high computing capacities) to produce day-ahead GHI probabilistic
621 forecasts should be favored compared to a deterministic (less demanding) approach. This
622 work opens the way to the assessment of the forecast value of each approach i.e. the benefit
623 (economical or others) gained from the use of these probabilistic forecasts in an operational
624 context.

625 **References**

- 626 [1] M. Pierro, M. De Felice, E. Maggioni, D. Mosere, A. Perottoc, Residual load probabilistic forecast for
627 reserve assessment: a real case study, *Renewable Energy* 125 (2019) 99–110. doi:10.1016/j.renene.
628 2019.12.056.
- 629 [2] Y. Zhu, Z. Toth, R. Wobus, D. Richardson, K. Mylne, The economic value of ensemble-based weather
630 forecasts, *Bulletin of the American Meteorological Society* 83 (2002) 73–83.
- 631 [3] R. Buizza, The value of probabilistic prediction, *Atmospheric Science Letters* 9 (2008) 36–42. doi:10.
632 1002/asl.170.
- 633 [4] M. Leutbecher, T. N. Palmer, Ensemble forecasting, *Journal of Computational Physics* 227 (2008)
634 3515–3539. doi:10.1016/j.jcp.2007.02.014.
- 635 [5] E. Lorenz, J. Hurka, D. Heinemann, H. Beyer, Irradiance forecasting for the power prediction of grid-
636 connected photovoltaic systems, *IEEE Journal of Selected Topics in Applied Earth Observations and*
637 *Remote Sensing* 2 (2009) 2–10.
- 638 [6] S. Alessandrini, L. Delle Monache, S. Sperati, G. Cervone, An analog ensemble for short-term probabilis-
639 tic solar power forecast, *Applied Energy* 157 (2015) 95–110. doi:10.1016/j.apenergy.2015.08.011.
- 640 [7] M. Zamo, O. Mestre, A. P., O. Pannekoucke, A benchmark of statistical regression methods for short-
641 term forecasting of photovoltaic electricity production. part ii: Probabilistic forecast of daily production,
642 *Solar Energy* 105 (2014) 804–816.
- 643 [8] P. Bacher, H. Madsen, H. A. Nielsen, Online short-term solar power forecasting, *Solar Energy*
644 83 (2009) 1772–1783. URL: <http://linkinghub.elsevier.com/retrieve/pii/S0038092X09001364>.
645 doi:10.1016/j.solener.2009.05.016.
- 646 [9] P. Lauret, M. David, H. Pedro, Probabilistic solar forecasting using quantile regression models, *Energies*
647 10 (2017) 1591. doi:10.3390/en10101591.
- 648 [10] E. B. Iversen, J. M. Morales, J. K. Møller, H. Madsen, Probabilistic forecasts of solar irradiance by
649 stochastic differential equations, *Environmetrics* 25 (2014) 152–164. doi:10.1002/env.2267.
- 650 [11] K. Bakker, K. Whan, W. Knap, M. Schmeits, Comparison of statistical post-processing methods
651 for probabilistic nwp forecasts of solar radiation, *Solar Energy* 191 (2019) 138–150. doi:10.1016/j.
652 solener.2019.08.044.
- 653 [12] S. Sperati, S. Alessandrini, L. Delle Monache, An application of the ecmwf ensemble prediction system
654 for short-term solar power forecasting, *Solar Energy* 133 (2016) 437–450. doi:10.1016/j.solener.
655 2016.04.016.
- 656 [13] L. Massidda, M. Marrocu, Quantile regression post-processing of weather forecast for short-term solar
657 power probabilistic forecasting, *Energies* 11 (2018) 1763. doi:10.3390/en11071763.
- 658 [14] P. Pinson, Adaptive calibration of (u,v)-wind ensemble forecasts, *Quarterly Journal of the Royal*
659 *Meteorological Society* 138 (2012) 1273–1284. doi:10.1002/qj.1873.
- 660 [15] P. Pinson, H. Madsen, Ensemble-based probabilistic forecasting at horns rev, *Wind Energy* 12 (2009)
661 137–155. doi:10.1002/we.309.
- 662 [16] C. Junk, L. Delle Monache, S. Alessandrini, Analog-based ensemble model output statistics, *Monthly*
663 *Weather Review* 143 (2015) 2909–2917. doi:10.1175/MWR-D-15-0095.1.
- 664 [17] T. Hamill, J. Whitaker, Probabilistic quantitative precipitation forecasts based on reforecast analogs:
665 Theory and application, *Monthly Weather Review* 134 (2006) 3209–3229. doi:10.1175/MWR3237.1.
- 666 [18] D. S. Wilks, Comparison of ensemble-mos methods in the lorenz ’96 setting, *Meteorological Applications*
667 13 (2006) 243. doi:10.1017/S1350482706002192.
- 668 [19] R. M. Williams, C. A. T. Ferro, F. Kwasniok, A comparison of ensemble post-processing methods
669 for extreme events, *Quarterly Journal of the Royal Meteorological Society* 140 (2014) 1112–1120.
670 doi:10.1002/qj.2198.
- 671 [20] T. Gneiting, A. E. Raftery, A. H. Westveld, T. Goldman, Calibrated probabilistic forecasting using
672 ensemble model output statistics and minimum crps estimation, *Monthly Weather Review* 133 (2005)
673 1098–1118. doi:10.1175/MWR2904.1.
- 674 [21] S. Lerch, L. Thorarinsdottir, T., Comparison of non-homogeneous regression models for probabilistic

- 675 wind speed forecasting, *Tellus A: Dynamic Meteorology and Oceanography* 65 (2013) 21206. doi:10.
676 3402/tellusa.v65i0.21206.
- 677 [22] S. Vannitsem, D. Wilks, J. Messner, *Statistical Postprocessing of Ensemble Forecasts*, Elsevier, 2018.
- 678 [23] P. Lauret, M. David, P. Pinson, Verification of solar irradiance probabilistic forecasts, *Solar Energy*
679 194 (2019) 254–271. doi:10.1016/j.solener.2019.10.041.
- 680 [24] D. V. Koenker, R., Confidence intervals for regression quantiles, *Journal of the Royal Statistical Society*
681 36 (1994) 383–393.
- 682 [25] V. Chernozhukov, I. Fernández-Val, A. Galicho, Quantile and probability curves without crossing,
683 *Econometrica* 78 (2010) 1093–1125. doi:10.3982/ECTA7880.
- 684 [26] L. Delle Monache, F. A. Eckel, D. Rife, B. Nagarajan, K. Searight, Probabilistic weather prediction with
685 an analog ensemble, *Monthly Weather Review* 141 (2013) 3498–3516. doi:10.1175/MWR-D-12-00281.1.
- 686 [27] S. Baran, S. Lerch, Combining predictive distributions for the statistical post-processing of ensemble
687 forecasts, *International Journal of Forecasting* 34 (2018) 477–496. doi:10.1016/j.ijforecast.2018.
688 01.005.
- 689 [28] M. Scheuerer, Probabilistic quantitative precipitation forecasting using ensemble model output statis-
690 tics: Probabilistic precipitation forecasting using emos, *Quarterly Journal of the Royal Meteorological*
691 *Society* 140 (2014) 1086–1096. doi:10.1002/qj.2183.
- 692 [29] R. Yuen, S. Baran, C. Fraley, T. Gneiting, S. Lerch, M. Scheuerer, T. Thorarinsdottir, ensem-
693 bleMOS: Ensemble Model Output Statistics, 2018. URL: [https://CRAN.R-project.org/package=](https://CRAN.R-project.org/package=ensembleMOS)
694 [ensembleMOS](https://CRAN.R-project.org/package=ensembleMOS), r package version 0.8.2.
- 695 [30] S. Yitzhaki, Gini’s mean difference: a superior measure of variability for non-normal distributions,
696 *Metron - International Journal of Statistics* 61 (2003) 285–316.
- 697 [31] T. E. Hoff, R. Perez, J. Kleissl, D. Renne, J. Stein, Reporting of irradiance modeling rela-
698 tive prediction errors, *Progress in Photovoltaics: Research and Applications* 21 (2013) 1514–
699 1519. URL: <https://onlinelibrary.wiley.com/doi/abs/10.1002/pip.2225>. doi:10.1002/pip.
700 2225. arXiv:<https://onlinelibrary.wiley.com/doi/pdf/10.1002/pip.2225>.
- 701 [32] D. Wilks, *Statistical Methods in the Atmospheric Sciences*, Academic Press, 2014.
- 702 [33] I. T. Jolliffe, D. B. Stephenson, *Forecast Verification: A Practitioner’s Guide in Atmospheric Science*,
703 Wiley, 2003.
- 704 [34] H. Hersbach, Decomposition of the Continuous Ranked Probability Score for Ensemble Pre-
705 diction Systems, *Weather and Forecasting* 15 (2000) 559–570. URL: [http://journals.](http://journals.ametsoc.org/doi/abs/10.1175/1520-0434(2000)015<0559:DOTCRP>2.0.CO;2)
706 [ametsoc.org/doi/abs/10.1175/1520-0434\(2000\)015<0559:DOTCRP>2.0.CO;2](http://journals.ametsoc.org/doi/abs/10.1175/1520-0434(2000)015<0559:DOTCRP>2.0.CO;2).
707 doi:10.1175/1520-0434(2000)015<0559:DOTCRP>2.0.CO;2.
- 708 [35] C. F. Coimbra, J. Kleissl, R. Marquez, Overview of Solar-Forecasting Methods and a Metric for
709 Accuracy Evaluation, in: *Solar Energy Forecasting and Resource Assessment*, Elsevier, 2013, pp.
710 171–194. URL: <http://linkinghub.elsevier.com/retrieve/pii/B9780123971777000085>.
- 711 [36] H. T. Pedro, C. F. Coimbra, M. David, P. Lauret, Assessment of machine learning techniques
712 for deterministic and probabilistic intra-hour solar forecasts, *Renewable Energy* 123 (2018) 191–
713 203. URL: <http://linkinghub.elsevier.com/retrieve/pii/S0960148118301423>. doi:10.1016/j.
714 [renene.2018.02.006](http://linkinghub.elsevier.com/retrieve/pii/S0960148118301423).
- 715 [37] K. Doubleday, V. V. S. Hernandez], B.-M. Hodge, Benchmark probabilistic solar forecasts:
716 Characteristics and recommendations, *Solar Energy* 206 (2020) 52 – 67. URL: [http://www.](http://www.sciencedirect.com/science/article/pii/S0038092X20305429)
717 [sciencedirect.com/science/article/pii/S0038092X20305429](http://www.sciencedirect.com/science/article/pii/S0038092X20305429). doi:[https://doi.org/10.1016/j.](https://doi.org/10.1016/j.solener.2020.05.051)
718 [solener.2020.05.051](https://doi.org/10.1016/j.solener.2020.05.051).
- 719 [38] J. Badosa, M. Haeffelin, H. Chepfer, Scales of spatial and temporal variation of solar irradiance on
720 reunion tropical island, *Solar Energy* 88 (2013) 42–56. doi:10.1016/j.solener.2012.11.007.
- 721 [39] N. Kalecinski, Processus de formation et d’étalement des nuages sur l’île de la Réunion: caractérisation
722 à partir de données issues d’observations satellite, sol et du modèle numérique de prévision AROME;
723 application à la prévision des énergies solaires., Ph.D. thesis, Ecole Polytechnique, 2015.
- 724 [40] T. E. Hoff, R. Perez, Modeling PV fleet output variability, *Solar Energy* 86 (2012) 2177–
725 2189. URL: <http://linkinghub.elsevier.com/retrieve/pii/S0038092X11004154>. doi:10.1016/j.

- 726 solener.2011.11.005.
- 727 [41] M. David, F. Ramahatana, P. Trombe, P. Lauret, Probabilistic forecasting of the solar irradiance with
728 recursive ARMA and GARCH models, *Solar Energy* 133 (2016) 55–72. URL: [http://linkinghub.
729 elsevier.com/retrieve/pii/S0038092X16300172](http://linkinghub.elsevier.com/retrieve/pii/S0038092X16300172). doi:10.1016/j.solener.2016.03.064.
- 730 [42] M. David, L. Mazorra Aguiar, P. Lauret, Comparison of intraday probabilistic forecasting of so-
731 lar irradiance using only endogenous data, *International Journal of Forecasting* 34 (2018) 529–
732 547. URL: <http://linkinghub.elsevier.com/retrieve/pii/S0169207018300384>. doi:10.1016/j.
733 ijforecast.2018.02.003.
- 734 [43] J. S. Whitaker, A. F. Loughe, The relationship between ensemble spread and ensemble mean skill,
735 *Monthly Weather Review* 126 (1998) 3292–3302. doi:10.1175/1520-0493(1998)126<3292:TRBESA>2.
736 O.CO;2.
- 737 [44] T. M. Hopson, Assessing the ensemble spread–error relationship, *Monthly Weather Review* 142 (2014)
738 1125–1142. doi:10.1175/MWR-D-12-00111.1.
- 739 [45] V. Fortin, M. Abaza, F. Anctil, R. Turcotte, Why should ensemble spread match the rmse of the
740 ensemble mean?, *Journal of Hydrometeorology* 15 (2014) 1708–1713. doi:10.1175/JHM-D-14-0008.1.
- 741 [46] C. N. Long, E. G. Dutton, BSRN Global Network recommended QC tests, V 2.0, Technical Report,
742 PANGAEA, 2010. URL: [https://epic.awi.de/id/eprint/30083/1/BSRN_recommended_QC_tests_
743 V2.pdf](https://epic.awi.de/id/eprint/30083/1/BSRN_recommended_QC_tests_V2.pdf).
- 744 [47] R. E. Bird, R. L. Hulstrom, Simplified Clear Sky Model for Direct and Diffuse Insolation on Horizontal
745 Surfaces, Technical Report, Solar Energy Research Institute, Golden, CO, 1981.

746 Acknowledgements

747 This work benefited from the support of the Energy4Climate Interdisciplinary Center
748 (E4C) of IP Paris and Ecole des Ponts ParisTech. It was supported by 3rd Programme
749 d’Investissement d’Avenir (ANR-18-EUR-006-02).

750 Appendix A. Data quality check

A quality check has been conducted for the observation data of each of the six studied sites. As the decomposition of irradiance into diffuse and direct has not been measured, the exhaustive set of BSRN recommended quality checks could not be conducted (see [46]), but only the first plot. It consists in the plot of measured irradiance versus solar zenith angle. The rarely reached limit is plotted in dashed line and the physical possible limit is plotted in solid line. The second check is a frequency histogram of the clear-sky index (k^*) for each site. k^* is defined as:

$$k^* = \frac{\text{Irradiance}}{\text{ClearSky Irradiance}} \quad (\text{A.1})$$

751 where the clear-sky irradiance is calculated with the Bird clear-sky model [47]. The maxi-
752 mum of the observed frequency is supposed to be at $k^* = 1$. The third check is a plot of the
753 k^* , only for clear-sky days. The morning data is reported by black dots and afternoon data
754 by red dots. From this plot, it is possible to see if clear-sky irradiances are well-reported
755 by the measurement data. If not, the line drawn by the dots is not straight. To extract
756 clear-sky days from the data, the process proposed in Badosa et al. [38] has been followed.
757 The last figure is a plot of the k^* for each hour and day of the year. It allows to detect

758 if systematical biases exist at some days/hours of the year. It also allows to easily detect
759 missing data.

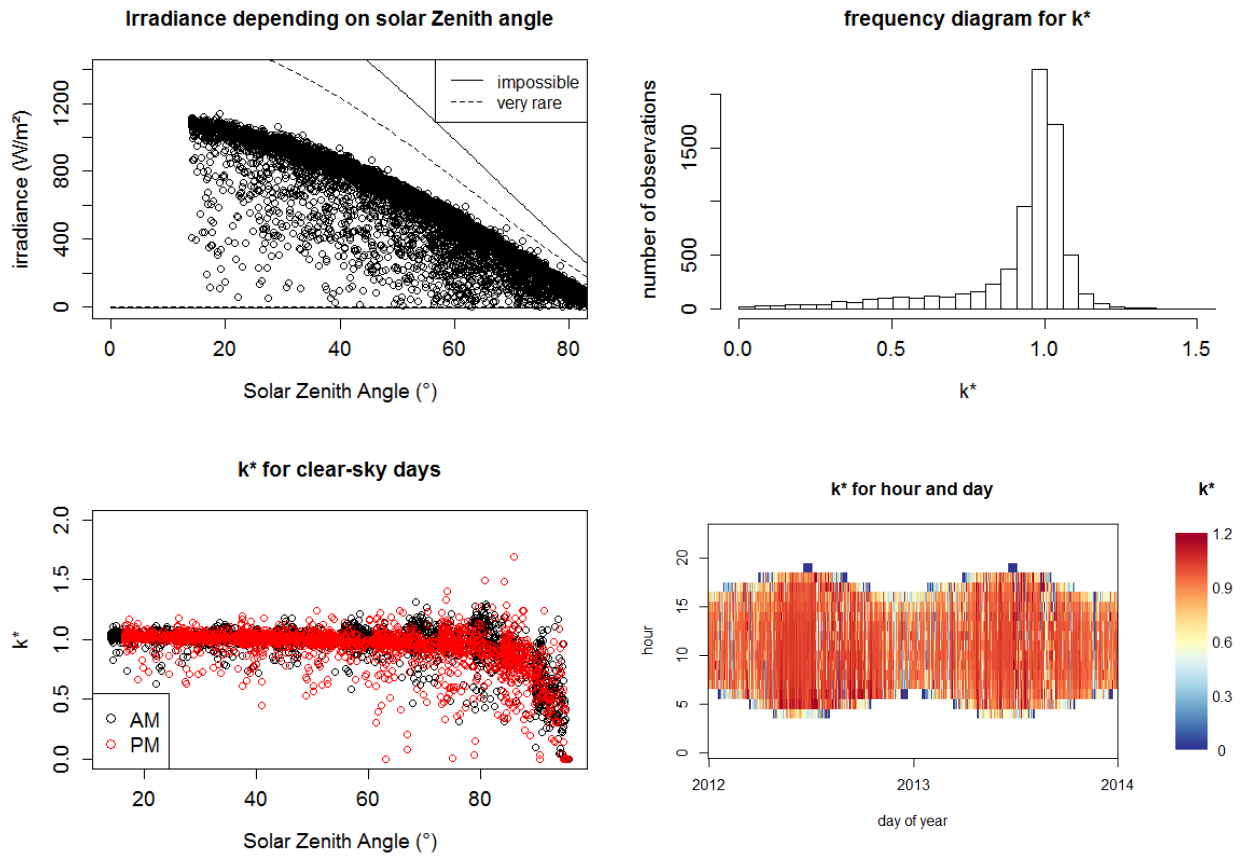


Figure A.10: Desert Rock

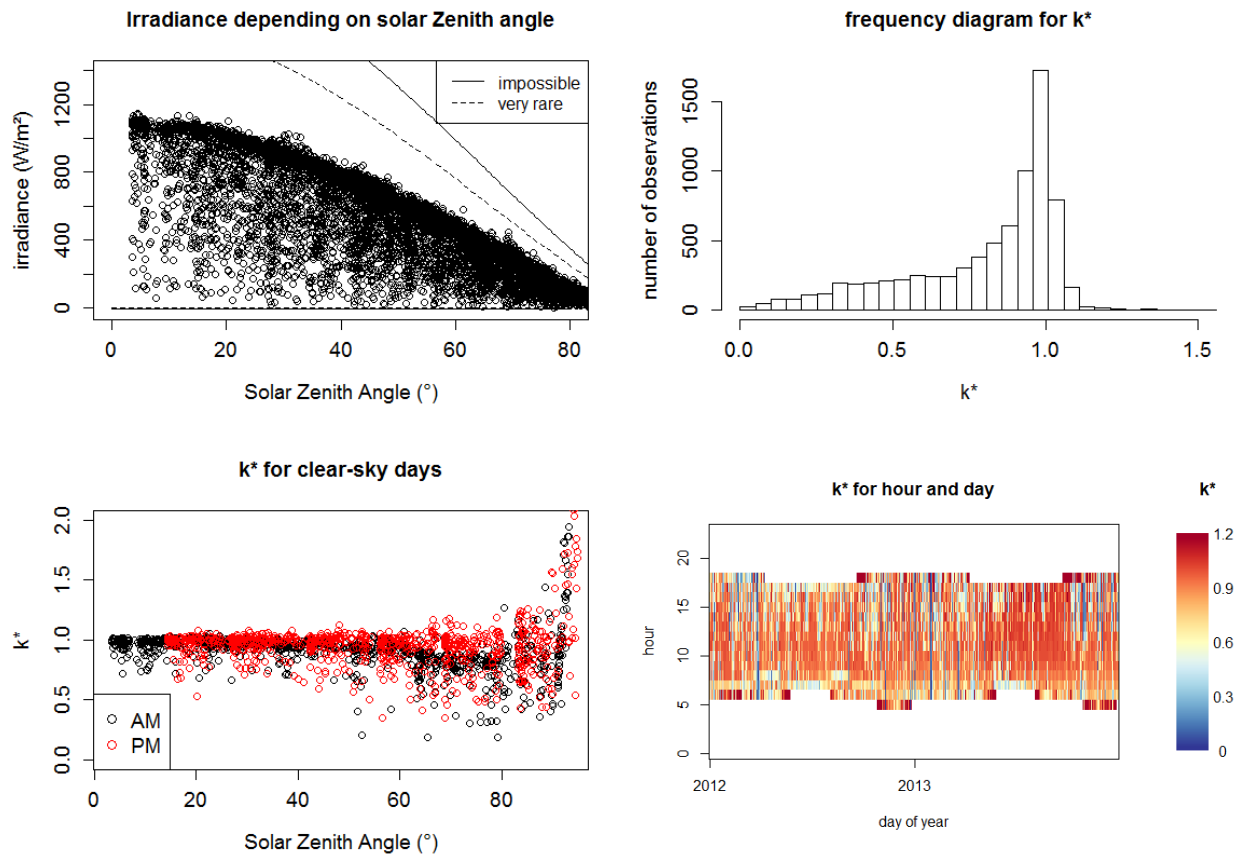


Figure A.11: Saint-Pierre

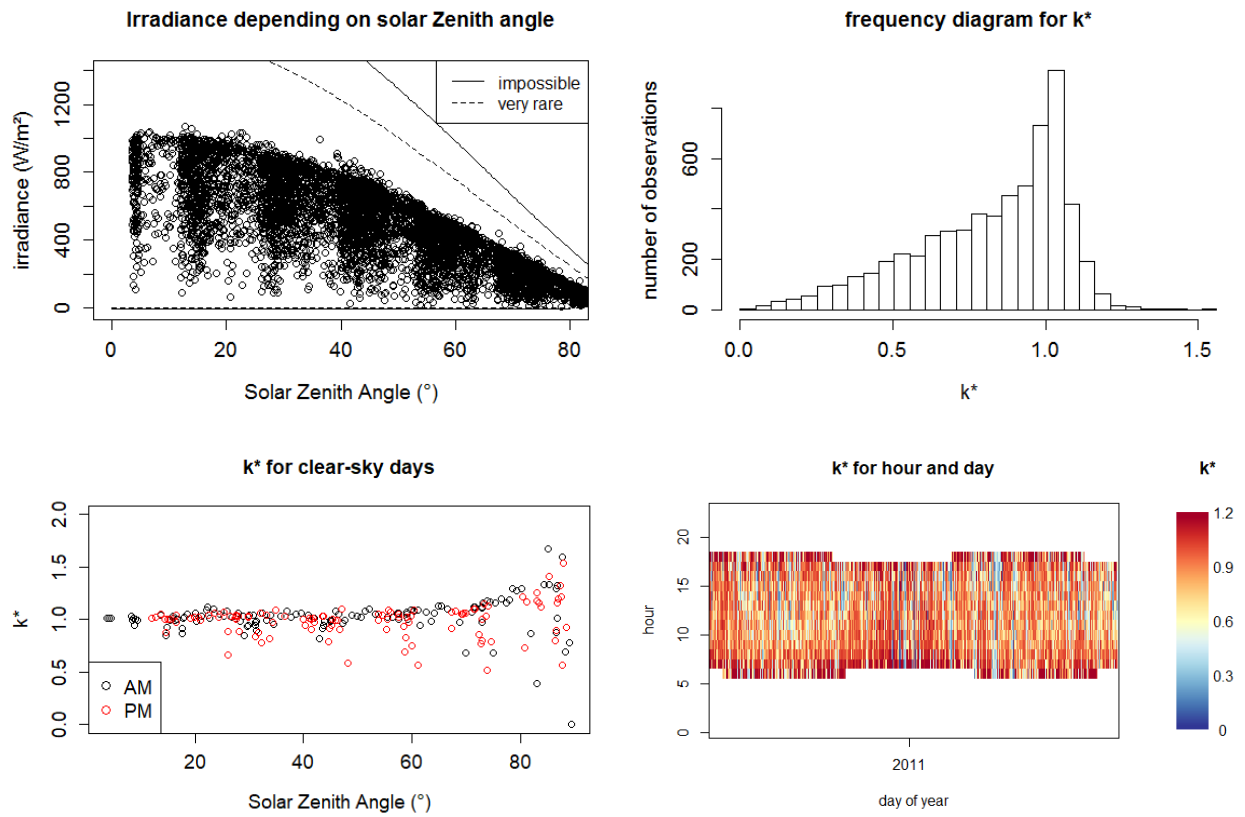


Figure A.12: Hawaii

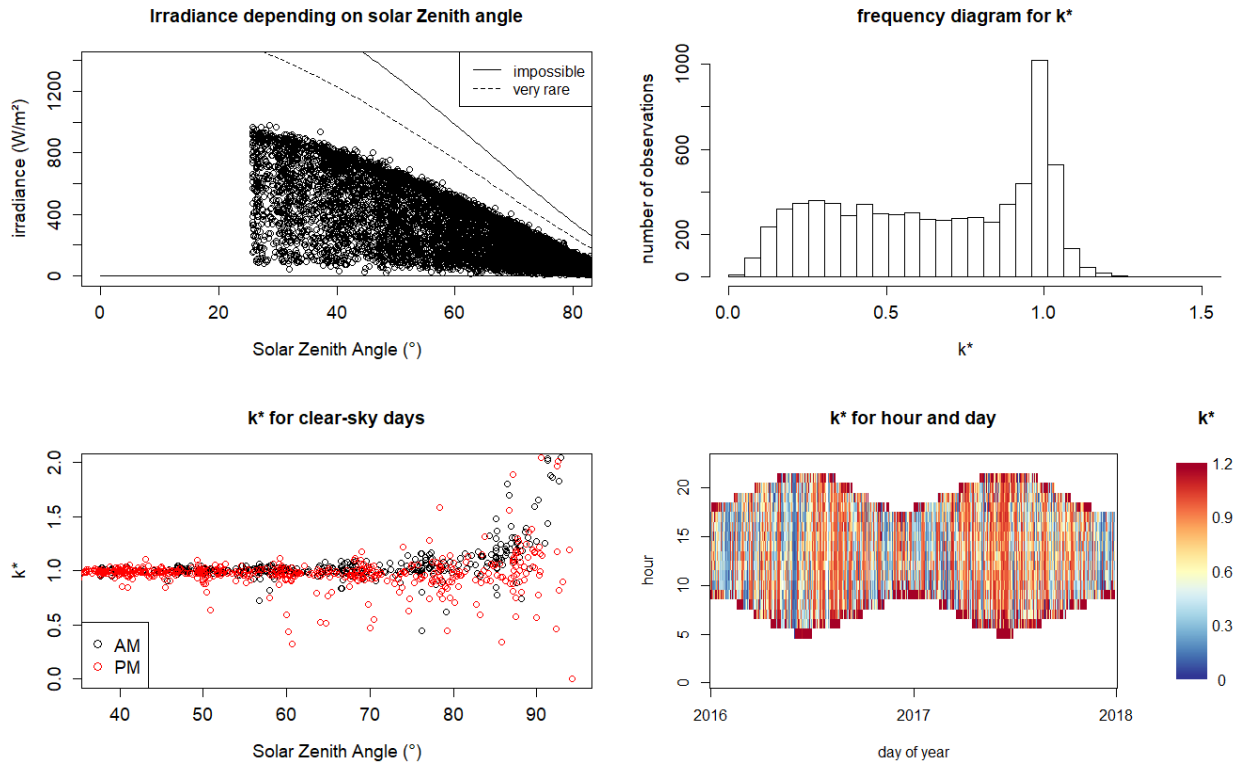


Figure A.13: Palaiseau

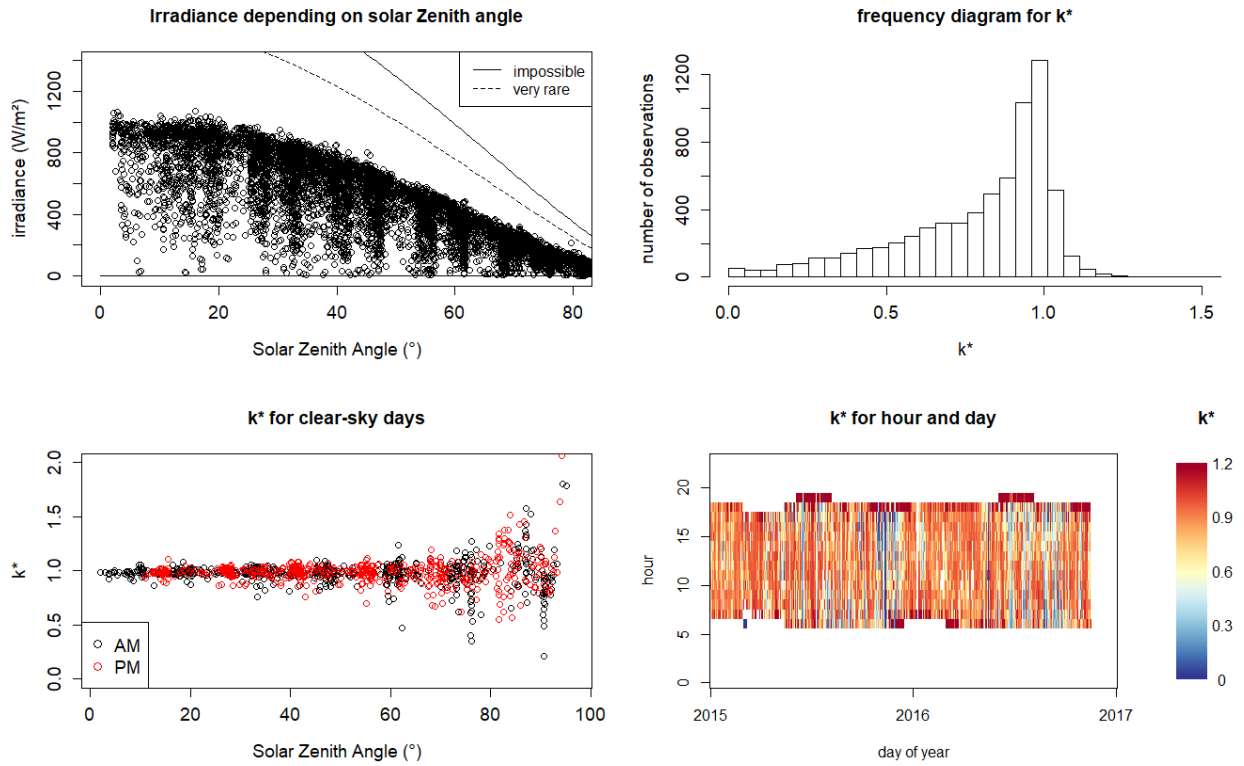


Figure A.14: Tiruvallur

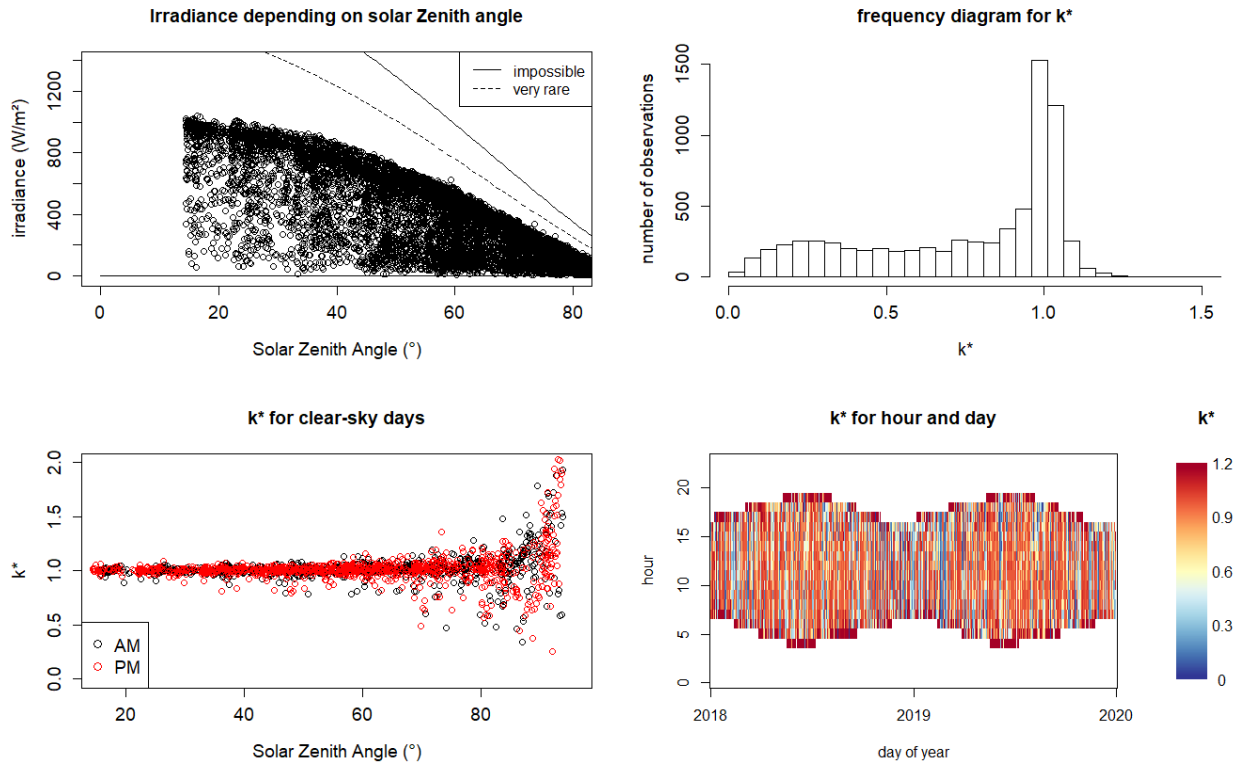


Figure A.15: Langley

760 No major issues have been detected concerning the six studied sites. For some sites
 761 (Tiruvallur, Langley, Saint-Pierre), it is possible to guess that some reflexions occur for
 762 extreme hours and some seasons. This leads to the phenomenon of overirradiance where k^*
 763 can easily reach a value of 4.

764 **Appendix B. Bias and standard deviation of EPS members distribution and**
 765 **observations for the six sites**

766 The definition of the probabilistic forecast presented in section 2.3.1 is often under-
 767 dispersive, and consequently obtains poor scores. The associated rank histograms usually
 768 get characteristic U-shapes, with overpopulated extreme ranks. In this section, we attempt
 769 to demonstrate why a calibration procedure is needed for raw forecasts. To this end, a
 770 comparison between members distributions and observation distributions depending on the
 771 level of forecasting has been conducted for the 2 first statistical moments. These plots
 772 show clearly under-dispersive raw ensembles. The standard deviations need to be corrected.
 773 The discrepancy between distributions of members and observations indicates a statistical
 774 inconsistency between observations and forecasts, and therefore a bad reliability, and justifies
 775 the use of calibration models.

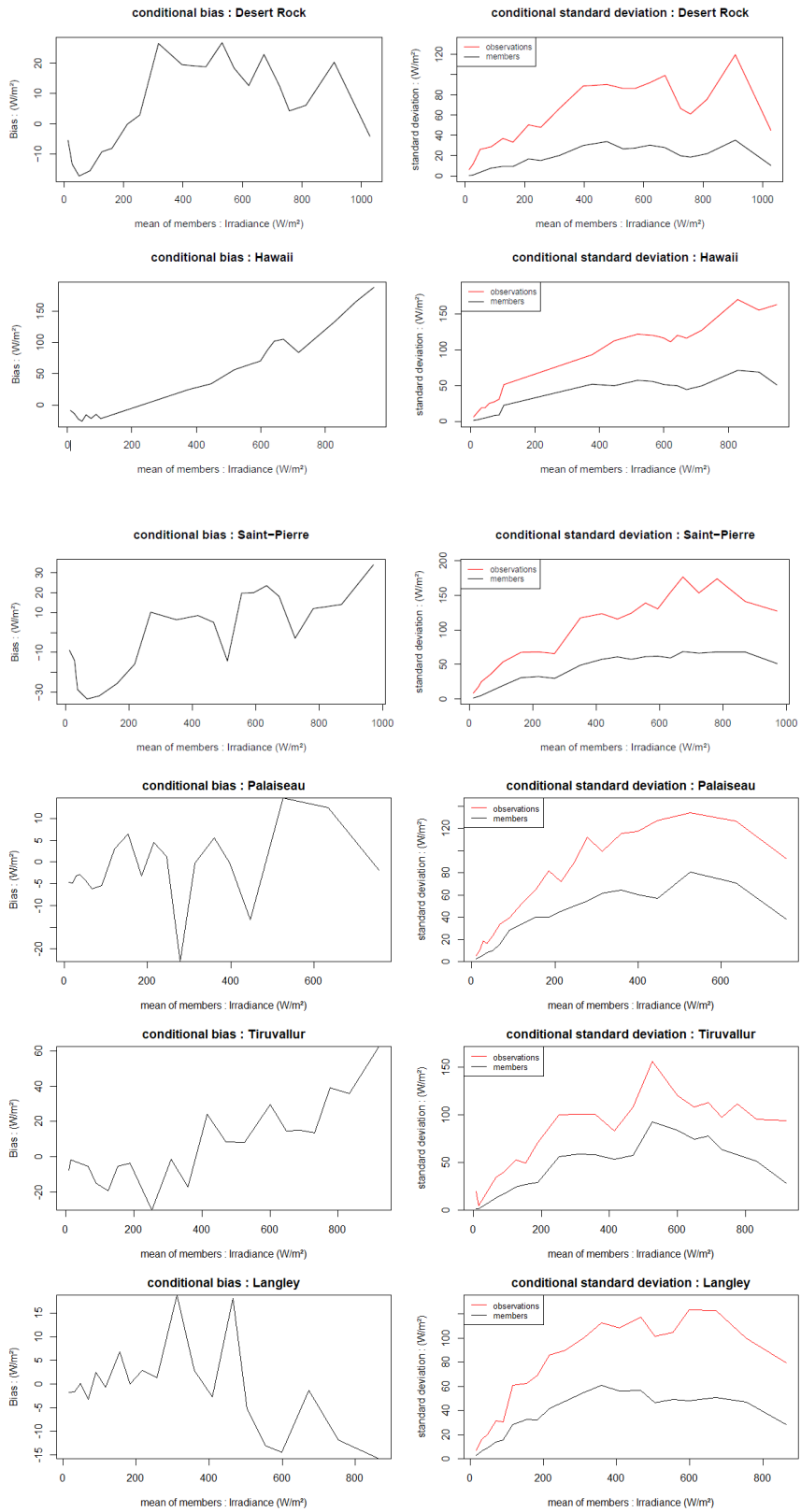


Figure B.16: Bias and standard deviation of EPS members distribution and observations for the six sites, depending on the level of forecasting

776 **Appendix C. Selection of the optimal α**

777 Figure C.17 presents the results related to the optimal selection of the parameter α . As
778 shown by Figure C.17, regardless of the site under study, the optimal value corresponds to
779 the minimum of the CRPS calculated on the training evaluation set.

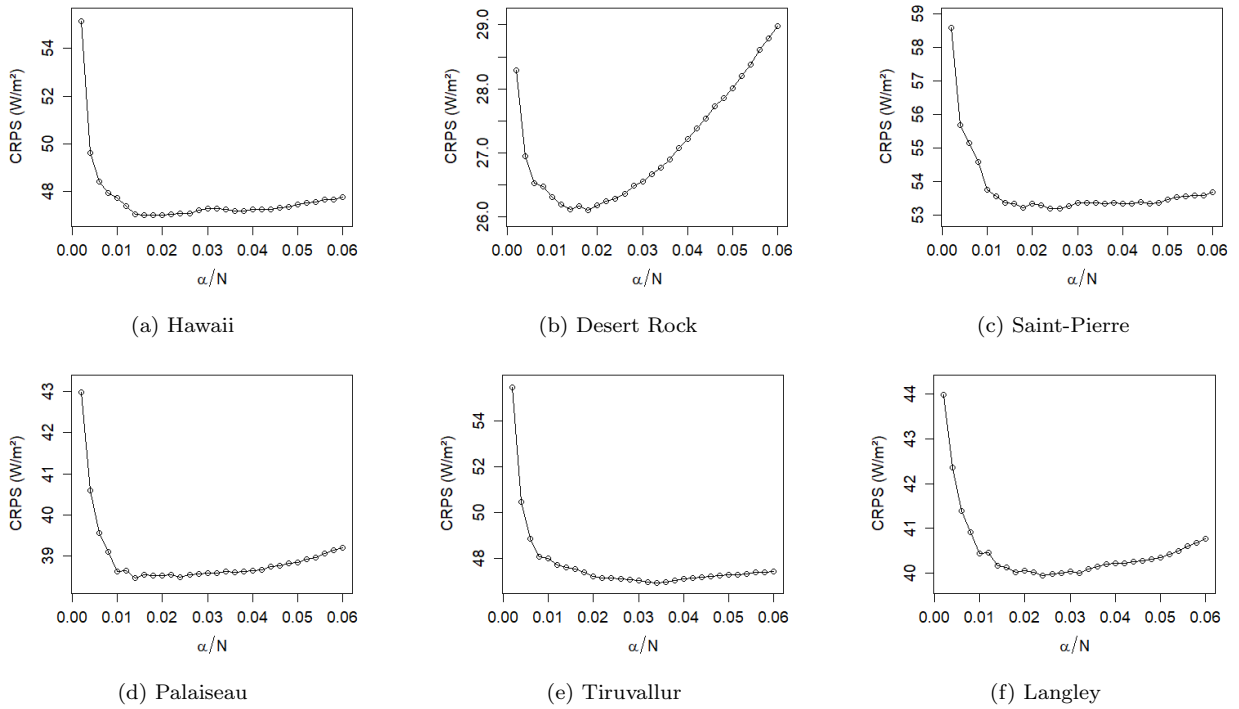


Figure C.17: Determination of the α . The optimal value corresponds to the minimum of the CRPS.